
# An Evaluation Of Detection and Recognition Algorithms To Implement Autonomous Target Tracking With A Quadrotor

Submitted in partial fulfilment
of the requirements of the degree of

BACHELOR OF SCIENCE (HONOURS)

of Rhodes University

O.H. Boyers

*Grahamstown, South Africa*
*November 2013*

## Abstract

Viola Jones face detection, Camshift, Haar-Cascades, quadrilateral transformation, fiducial marker recognition and Fisherfaces are algorithms and techniques commonly used for object detection, recognition and tracking. This research evaluates the methodologies of these algorithms in order to determine their relative strengths, weaknesses and suitability for object detection, recognition and tracking using a quadrotor. The capabilities of each algorithm are compared to one another in terms of their effective operational distances, effective detection angles, accuracy and tracking performance. A system is implemented that allows the drone to autonomously track and follow various targets whilst in flight. This system evaluated the feasibility of using a quadrotor to provide autonomous surveillance over large areas of land where traditional surveillance techniques cannot be reasonably implemented. The system used the Parrot AR Drone to perform testing owing to the drone's on board available sensors that facilitated the implementation of computer vision algorithms. The system was successfully able evaluate each algorithm and demonstrate that a micro UAV like the Parrot AR Drone is capable of performing autonomous detection, recognition and tracking during flight.

**ACM Computing Classification System Classification**

Thesis classification under the ACM Computing Classification System (1998 version, valid through 2013):

**I.2.9** [Robotics]: Autonomous vehicles, sensors

**I.4.0** [General]: Image processing software

**I.4.8** [Scene Analysis]: Tracking, colour

**I.5.4** [Applications]: Computer vision

**General-Terms:** Autonomous Robot, Algorithms, Performance

## Acknowledgements

I would like to thank my supervisor, Mr James Connan for his help and support with this project. His broad knowledge in the field of image processing and scientific writing equipped me with the integral tools and direction needed to complete this thesis. I would like to acknowledge the financial and technical support of Telkom, Tellabs, Stortech, Genband, Easttel, Bright Ideas 39 and THRIP through the Telkom Centre of Excellence in the Department of Computer Science at Rhodes University. Lastly, but most importantly, I would like to thank my incredible parents, Kevin and Marion. For without their unwavering support throughout the course of my university career none of this would have been possible.

# Contents

# List of Figures

# List of Tables

# Chapter 1

# Introduction

There are many existing applications of computer vision and automation in the field of robotics. These range from medical applications, such as high precision surgical equipment, to military applications, such as targeting and surveillance systems. The idea of creating machines that can perform complex tasks without human assistance has great implications in many fields. An autonomous or remote controlled vehicle can enter areas that humans cannot. This can allow humans to survey and interact with environments subject to radioactivity, highly contagious diseases and war. More importantly, this enables one to carry out tasks without risking the loss of human life.

Computer vision is one of many techniques that can be used to implement autonomy in robots. Computer vision aims to recreate the human sense in order to extract valuable information from an image or a series of images. The information extracted from the images can then be used to perform various functions such as determine which direction a vehicle should move to avoid collisions or to decide on an algorithm to execute. Computer vision uses various image processing procedures to obtain information from its image feed. The information that can be extracted from these images can often be more useful than the information a human can derive from the same images. This can be attributed to the use of machinery that surpasses human ability.

There are many applications of computer vision in surveillance. Closed circuit television systems are widely used to monitor environments that maintain a high level of security such as airports and embassies. These systems use computer vision to monitor persons accessing the premises and to detect threats such as unattended baggage. These systems can be easily implemented in small environments but becomes significantly more difficult over large areas such as nature reserves. The

size of a nature reserve makes traditional CCTV-like surveillance systems impossible to implement owing to the high cost of equipment, maintenance and staff. How then can the managers of a nature reserve protect the reserve from threats such as poachers? A conceived solution to this problem is to use autonomous aerial drones to survey these large areas. The drones could use computer vision to detect threats. Furthermore, the drones could track detected threats in order to assist the appropriate authorities in quelling the threat.

## 1.1 Problem Statement and Research Goals

The aim of this research project is to create a system that tests whether it is feasilble to use aerial drones to autonomously detect, recognise and track a target using computer vision. The drone will perform detection, recognition and tracking using an on board camera which streams a video feed to a client application. The client application will apply image processing procedures to the video feed and return flight commands to the drone based on information extracted from the video. The main constraint on detection, recognition and tracking algorithms is that they need to be efficient enough to be used in real-time. The end result of this project will be a system that allows an aerial drone to autonomously detect, recognise and track a target.

### 1.1.1 Research Question

- What are the relative strengths and weaknesses of the detection and recognition algorithms?
- Are these algorithms suitable for tracking using a quadrotor drone?
- Can a system be built that will take the live video feed from the drone and perform basic tracking in an indoor environment?

### 1.1.2 Objectives

In order to answer these research questions, the following objectives need to be met:

- Detect various targets using the on board camera of an aerial drone.
- Recognise detected targets using computer vision algorithms.
- Test and compare the capabilities and performance of each detection and recognition algorithm.
- Implement an algorithm that can send flight commands to a drone in order to autonomously track a detected object.

- Determine whether it is feasible to use aerial drones to autonomously perform target detection, recognition and tracking.

## 1.2 Thesis Organisation

The subsequent chapters of this thesis are organised as follows:

**Chapter 2** discusses literature on different types of drones that exist, their attributes and methods of flight automation. This literature consists of previous research conducted in these areas as well as the various options available for designing the proposed system.

**Chapter 3** discusses various application programming interfaces (APIs) that can be used to interface with the AR Drone. This assisted in determining which API was best suited to carry out target detection, recognition and tracking

**Chapter 4** covers the software tools and algorithms used to perform tracking and recognition functions.

**Chapter 5** covers the implementation of CamShift tacking, Haar-Cascade tracking, fiducial marker/glyph recognition and the tracking implementation.

**Chapter 6** details the various tests performed with the AR Drone to assess the capabilities of each algorithm with respect to detection, tracking and recognition. Furthermore, it discusses the strengths and weaknesses of each algorithm according to the results obtained from tests.

**Chapter 7** gives a brief summary of this thesis, revisits its goals and discusses work that can be done in the future to elaborate on this system.

# Chapter 2

# Background

### Introduction

Since this project is primarily focused on the automation of aerial drones, it is necessary to give a brief background on the different types of drones that already exist and some of their applications. The following sections will look at the various types of drones and their practical applications. The components of a drone are discussed as well as the impact that each component has on the drones functionality.

## 2.1 Drones

Drones are unmanned vehicles that can either operate autonomously, or via control from a remote location. There are various types of drones such land based, aerial based or water based drones. This section will focus on aerial drones as they are the most mobile and effective tools for target detection, recognition and tracking. UAVs are used in various fields to perform many tasks. Small UAVs such as the quadrotor are most commonly used in the field of aerial imagery such as photographing property for real estate companies or for filming purposes. Drones have even been used to survey areas that have been flooded to determine the extent of the flood and to look for people that have been stranded. The military even make use of drones as they have an advantage over traditionally piloted air vehicles. UAVs allow the military to carry out dangerous operations without endangering the life of a pilot. This allows operations to be carried out in areas of conflict, areas of infection or remote locations without placing a pilot at risk.

### 2.1.1 Fixed wing Vs Rotary wing

UAV's come in two forms: fixed wing and rotary wing. Fixed wing UAV's are able to fly much further distances than their rotary wing counterparts and can travel at higher speeds. This however comes at the expense of requiring a runway for take-off and landing. Rotary wing UAV's on the other hand have the ability to take-off and land vertically, hover and perform more complicated flying manoeuvres than the fixed wing UAVS. This limits the range and speed of the rotor wing UAVs. The rotor wing UAV is also mechanically complex to build (Crew, 2013).

The rotary wing's ability to hover allows the UAV to hold a fixed position. This allows it to take video footage whilst loitering close to a target rather than having to circle/orbit the target like a fixed wing UAV. This also allows the rotary wing to travel to a destination and land in a position where it can monitor its target. After landing, the UAV can turn its engine off to conserve battery power while its on board audio and visual sensors can continue to capture information. This is call the "perch and stare" (Danko *et al.*, 2005) and is found very useful in reconnaissance operations. The rotary wing UAV is also useful when being used to deliver payloads to precise locations as it can travel to the target destination, hover and then dump its payload. When delivering payloads with a fixed wing UAV, the forward momentum of the craft will cause the dropped payload to move a large distance whilst falling and will tumble once it has made contact with the ground. Rotary wing UAVs can also collect payloads easily owing to their ability to hover in a fixed position (Crew, 2013) .

UAVs have started to become widely used devices in the fields of research and recreation. This popularity has driven recent advances in technology in the fields of batteries, wireless communication and solid state devices. This has allowed low cost UAVs to become readily available for many applications in military, civil and scientific sectors. Low flying rotary UAVs can be used for scientific data gathering, nature reserve monitoring, surveillance for law enforcement and military reconnaissance to name a few. The US Military (Mayer, 2009) are currently using UAVs such as the Predator Drone and the Global Hawk which are very large and extremely expensive vehicles that have limited autonomy. On the other hand, small UAVs and micro UAVs that are being developed primarily in universities and research environments face very different problems than their larger counterparts. These are problems such as finding strong lightweight vehicle platforms, making use of components that demand small amounts of power and implementing easily understandable human interfaces. These small UAVs also require increased autonomy including path planning, trajectory generation

and tracking algorithms (Beard *et al.*, 2005).

## 2.2 Attributes of drones

This section will look at various attributes of drones. Certain attributes need to be considered when deciding on which drone will be used for the implementation of target detection, recognition and tracking. These attributes include the weight, endurance, range, maximum altitude, wing loading and engine type.

### 2.2.1 Weight

UAVs can range drastically in weight from the micro UAVs that can weigh up to 5kgs such as the Dragon Eye in Figure 2.1 to the huge Globo Hawk which weighs over 11 tonnes. The lighter UAVs tend to make use of electric motors whereas the heavier UAVs use turbo fan or jet engines (Arjomandi *et al.*, 2007). This project requires a light weight drone that can be operated indoors for testing purposes.

Figure 2.1: The Dragon Eye. A micro UAV (Arjomandi *et al.*, 2007)

### 2.2.2 Endurance and Range

These two attributes are related as the longer a UAV can stay airborne and maintain cruising speed, the more distance it can cover, provided the drone is still within communication range. It is important to use endurance and range to classify UAVs, as different types of UAVs are required to perform different tasks. These tasks may be carried out in areas that are close the launch site or large distances away. The drone's range also determines how regularly it needs to refuel or recharge. Most drones have to be grounded to refuel or recharge and this affects operation times. Larger drones such as the Global hawk have the ability to refuel in the air but this will still come at the expense of time. The low endurance UAVs such as the AR Drone has an airtime of up to 20 minutes and is normally used for short distance operations. UAVs with a high endurance can stay airborne for more than 24 hours and can have a range of up to 22000 km (Arjomandi *et al.*, 2007). The endurance a drone will require for this project need not be more than 15 minutes of flight time as this will be sufficient to test detection, recognition and tracking concepts. The range need not be more than 20 meters as testing will be performed within a short distance of the controlling client application.

### 2.2.3 Maximum altitude

This is an important characteristic to consider when selecting a drone as some operations require drones to avoid detection by maintaining a low visibility at high altitudes. This prevents the drone from being detected and destroyed by the enemy in military situations. Altitude also needs to be considered when a drone is used for imaging terrain as a high altitude is required to capture as much terrain as possible. Low altitude UAVs such as the AR Drone can fly at heights of up to 100m. High altitude drones such as the Darkstar 2.2 and Predator B can reach heights over 45,000ft. There is concern however that these high altitude UAVs may interfere with other commercial or military aircraft. To mitigate these risks, drones that fly in populated airspaces are programmed with advanced collision avoidance systems (Arjomandi *et al.*, 2007). This project will require a drone that can operate at low altitude for monitoring and testing purposes.

Figure 2.2: The Darkstar on display at a USAF base

### 2.2.4 Wing loading

Wing loading refers to the ratio of the weight of an airplane to its wing area. This affects how much of a load a UAV can carry and what speed the aircraft needs to travel to carry this load. An aircraft produces more lift per unit area of wing the faster it flies. This allows smaller aircraft to carry the same load as large aircraft so long as the small aircraft travels at a higher speed. This forces heavier loaded aircraft to take-off and land at higher speeds and decreases the ability of the aircraft to manoeuvre (Morris, 1997).

### 2.2.5 Engine type

UAVs can be classified by their engine type and have several variations such as piston, rotary, turboprop, electric and propeller. The weight of the plane is closely tied to the engine type as the bigger the plane is, the more power is needed to create the required amount of lift. Smaller UAVs tend to make use of lighter electric engines while heavier more industrial UAVs use piston engines. A UAVs engine can also determine the drones range and endurance.

## 2.3 Drone Selection

Taking into consideration the above UAV classification characteristics, the ideal aircraft for this project would be a light weight micro UAV under 5kgs. The endurance and range of the aircraft will only need to be enough to satisfy a proof of concept. This will be a flight time of approximately 15 minutes and a range of up to 20m. The maximum altitude need only be a few metres to test flight movements. A vertical take-off and landing system (VTOL) is required to perform testing in relatively small environments. Whilst testing this proof of concept no load will need to be carried by the drone but a working solution of an anti-poaching drone will need to have a load carrying ability to accommodate additional sensors and batteries to extend flight time. The engine of choice for this proof of concept is an electric engine as a small UAV will not require very large amounts of power to lift it and an electric engine is easily rechargeable. The Parrot AR Drone fits all of the requirements for this project and will be the drone used in testing.

## 2.4 The AR Drone Quadrotor

The Parrot AR Drone is a micro UAV that was created primarily for the home entertainment and video games sector. The drone was launched in 2010 and has since gone way beyond conventional use and has been considered in both military and civilian applications. The AR Drone has attracted a lot of attention from the academic world. The drone's light weight, low cost and capability to manoeuvre with agility has made the AR Drone the perfect test subject for many projects. The AR Drone is capable of hovering, rapid forward flight and comes with a pilot platform that is easy to control. The piloting of the AR Drone can be performed via applications on various smart phones which give users access to high level orders. These orders are handled by an automatic controller that deals with the complexity of the low level sub systems (Bristeau *et al.*, 2011).

The sections below assess the different components of the AR Drone. These components include the AR Drones engine, power source, software, hardware and various sensors.

### 2.4.1 Engines

The AR Drone makes use of brushless engines that are controlled by a micro controller to power the rotors. The AR Drone can detect whether all four engines are working and if any have stopped. This is to prevent repeated shocks to the engine if the propeller encounters and obstruction whilst rotating.

If an obstruction to any propeller is detected, the AR Drone stops all engines (Stephane Piskorski, 2011).

### 2.4.2 LiPo batteries

The AR Drone makes use of a charged 100mAh, 11.1V LiPo battery to fly. The battery's charge is determined full when at 12.5V and low when at 9V. The drone monitors the voltage of the battery and displays it to the user as a percentage so that flight decisions can be made accordingly. When the drone detects the battery is at a low voltage, it sends a warning message to the user before landing automatically. Should the voltage of the battery reach a critical point at any stage, the AR Drone will shut down immediately to prevent the drone from behaving in any unexpected fashion (Stephane Piskorski, 2011).

### 2.4.3 Accelerometer, gyrometers and processors

The AR Drone's sensors are located below the central hull of the drone. The AR Drone has a six degrees of freedom, micro electro-mechanical system (MEMS) based, miniaturized inertial measurement unit (Stephane Piskorski, 2011). This measurement unit provides the drone's software with pitch, roll and yaw measurements. The measurement unit also contains a three axis accelerometer, a two axis roll and pitch gyro meter and a single axis yaw gyro meter (Dijkshoorn, 2012). The AR Drone also has two cameras, a motherboard, which holds two processors and sonar. One of these processors is used to gather data from I/Os. The other is used to run all the algorithms that the drone needs to maintain flight stability and process images (Bristeau *et al.*, 2011). The accelerometer is a BMA150 made by Bosch Sensortec. "The accelerometer outputs g-forces (acceleration relative to free-fall) as a quantity of acceleration" (Dijkshoorn, 2012). This measurement is based on the phenomenon that the observed weight of an object changes whilst that object is accelerating. The MEMS accelerometer makes use of three plates on separate axes and can measure acceleration in the direction of the axis. This ability of the accelerometer to measure gravity allows it to be used as a tilt sensor. The gyro meters measures angular velocity in degrees per second to detect tilt in the X(roll),Y(pitch) and Z(yaw) as depicted in Figure 2.3.

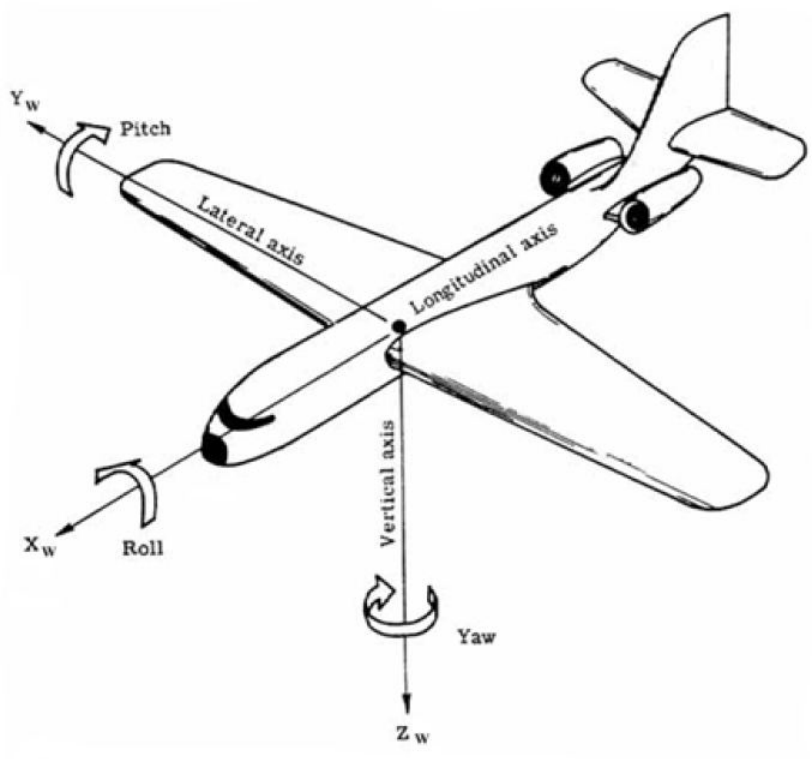


Figure 2.3: Roll Pitch Yaw

### 2.4.4 Motherboard

The mother board of the AR Drone has various components embedded in it. The Parrot P6 processor (32bits ARM9 core, running at 468MHz), a Wi-Fi chip, a camera that is oriented vertically and and connector that runs to the forward facing camera of the drone. The drone makes use of a Linux based real time operating system whose calculations are performed on the Parrot P6 processor. The P6 processor is also tasked with retrieving the flow of information from both video cameras.

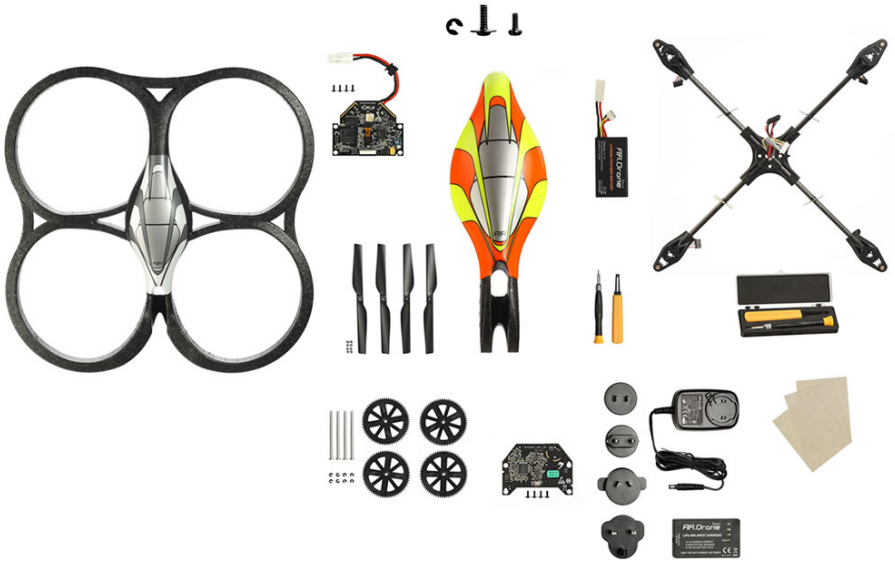

Figure 2.4: Quadrotor Components (AR.Drone2.0, 2013)

### 2.4.5 Cameras

The AR Drone has two built in CMOS cameras. One downward facing and one forward facing. Both can support a live video stream at up to 15 frames per second. The front facing camera has a 93 degree field of view and has a VGA resolution (640x480). This front facing camera is used to detect other drones during multiplayer games and to stream video footage back to the controlling device such as tablet device or smart phone. The downward facing camera has a field of vision of 64 degrees and a resolution of 176x144. The downward facing camera has a frequency of 60 frames per second so that the blur of motion is reduced and thus improves the flight algorithms that make use of this camera. However, when streaming the video from this camera the frequency is still streamed at 15 frames per second. Both cameras play a pivotal role in the AR Drone's ability to fly and on board intelligence (Dijkshoorn, 2012).

### 2.4.6 Ultrasound altimeter

The ultrasound sensor provides the AR Drone with altitude measurements so that automatic altitude stabilization can take place. The altitude measurement also assists with the vertical speed control algorithm. The ultrasound altimeter is attached to the bottom of the drone and points down in order to measure the distance between the drone and the floor as depicted in Figure 2.6. The ultrasound

waits for its transmitted signal to echo back to it and then determines the distance between the object and the sensor using the amount of time it took the echo to return. The distance is computed using the speed of sound where c $\approx$ 343m/s is the speed of sound in air.

$$d = \frac{c \times t}{2}$$

Figure 2.5: Calcualting distance using the speed of sound (Dijkshoorn, 2012)

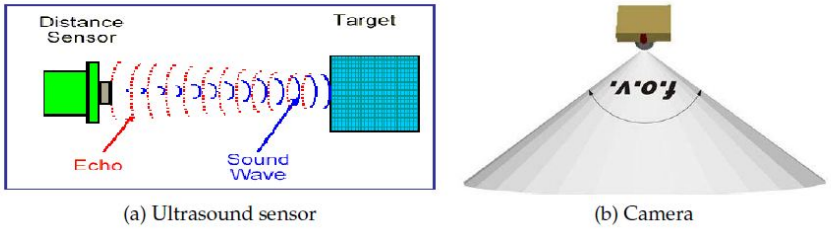


(a) Ultrasound sensor (b) Camera

Figure 2.6: Ultrasound altimeter (Stephane Piskorski, 2011)

### 2.4.7 Embedded software

The operating system (OS) that the AR Drone uses is a custom embedded Linux real time OS. The OS simultaneously manages threads pertaining to: "Wi-Fi communications, video data sampling, video compression (for wireless transmission), image processing, sensors acquisition, state estimation and closed-loop control" (Bristeau *et al.*, 2011).

## 2.5 Flight Automation

### Introduction

Flight automation is an important factor to consider when implementing a target detection, recognition and tracking system. Automation will allow a drone to execute various directives when human control is not available.

Flight automation using the AR Drone can be performed by using the images from the cameras to implement computer vision control, create three dimensional (3D) models or use sensor measure-

ments to make flight decisions. As the testing of our AR Drone will be taking place mainly indoors, the use of GPS has been ruled out as a sensor to facilitate autonomous flight. The following sections will describe various possible flight automation implementations including 3D modelling, the simultaneous localisation and mapping algorithm and image based mapping.

### 2.5.1 3D modelling

3D modelling involves creating a mathematical representation of any 3D object or surface. The 3D model can be displayed as a two dimensional image using 3D rendering via 3D modelling software. 3D models provide more information than 2D models as they provide a measurement of depth. 3D models are created by combining vision technology and laser range determining data in a single representation. These representations can map objects such as stairs and windows that are unable to be represented in 2D mapping (Biber *et al.*, 2004).

### 2.5.2 Simultaneous Localization and Mapping (SLAM) Algorithm

A micro UAV like the AR Drone with a vision based SLAM could be the key to creating a GPS free autonomous navigation tool for modern day buildings and outdoor areas (Çelik *et al.*, 2009). The SLAM algorithm builds a map of an unknown environment within which it will navigate. It can also update a known environment should there be any changes. The mapping is performed whilst the drone keeps track of its current position. The mapping is executed using a set of information the drone consistently gathers from its various sensors. This information can then be used to create a 2D or 3D environment.

### 2.5.3 Image based mapping

Image based mapping is now a popular alternative to 3D mapping techniques. This technique uses geometric representations to map an environment. The environment is mapped by creating "photo-realistic graphics and animations of scenes in real-time (Biber *et al.*, 2004)." Currently, panoramic views and virtual environments are the most well-known products of image-based rendering. Google street view is an example of these photorealistic graphic environments. In these virtual environments a user is able to look around the environment freely and can zoom into areas of the image. To allow this complete degree of freedom a plenoptic function has to be sampled. This is a six dimensional function that requires a large amount of memory. In one particular implementation of this image based mapping, an area of $81\text{m}^2$ was mapped using approximately 10,000 images (Biber *et al.*, 2004).

### Summary

After considering the above flight automation implementations as well as the capabilities of the AR Drone it was decided to use an image based approach to automation. The AR Drone's on board camera will be used to gather images which will be processed to make flight decision.

## 2.5.4 Related work in visual and non-visual flight automation

This section covers related work in the field of flight automation and mapping. The sections include visual based navigation, non-visual based navigation, stability and control and navigation patterns.

### Introduction

It is necessary to consider related work in visual and non-visual flight automation so that informed decisions can be made when implementing the navigation of the AR Drone. Related work also illustrates the capabilities of the UAVs and can highlight the importance of certain aspects of flight navigation automation.

## 2.5.5 Visual based navigation

Using micro UAVs that use image based navigation techniques is an efficient navigation technique. This is because a vision based navigation system can provide long range sensing with low power demands. The study by Nicoud et al. (2002) discusses UAV design trade-offs for indoor aerial vehicles (Nicoud & Zufferey, 2002). These trade-offs address the issues of aerodynamics, the weights of UAVs, wing, propeller and motor characteristics. The paper proposes a methodology to optimize the motor/gear/propeller system from which a UAV with low power demands is created. Mejias et al. (2006) used a vision based navigation system to land a UAV whilst avoiding power lines (Mejias *et al.*, 2006). The vision system here allows the UAV to make flight decisions based on its 2D position in relation to a feature or set of features in the image. The features used here were those of power lines and their various arrangements. Zingg et al. (2011) discuss a vision based algorithm for flying a micro UAV in corridors using a depth map (Zingg *et al.*, 2010) (Bills *et al.*, 2011). This approach uses the optical flow of images from cameras mounted on the UAV to avoid collisions.

## 2.5.6 Non-visual based navigation

Non-visual navigation methods make use of sensors such as laser range scanners, sonar and infra-red. The study by Roberts et al. (2009) made use of ultra-sonic and infra-red sensors to fly a quadrotor

in an environment where strict requirements needed to be fulfilled (Roberts *et al.*, 2009). This paper proved it viable for a small, lightweight, large range UAV with infra-red sensors to be able to navigate effectively in circumstances of tilting, misalignment and ambient light changes. It was able to overcome these conditions whilst still maintaining range and directional accuracy in the 6x7m environment in which tests were performed. This implementation however could not perform long range sensing beyond these dimensions. The study by Achtelik et al. (2009) used a laser rangefinder and a stereo camera to implement navigation in unstructured and unknown indoor environments using a quadrotor (Achtelik *et al.*, 2009). These sensors are effective in determining the helicopter's relative motion and velocity. The number of sensors that a quadrotor can use is limited by the payload the UAV can carry. This restricts the capability of UAVs and custom quadrotors are often built to handle a heavy load of sensors or additional batteries for those that are power demanding. Most micro UAVs only have the ability to carry small payloads and power efficient sensors like a camera (Bills *et al.*, 2011).

### 2.5.7 Stabililty and control

Vision based algorithms have been used for flight stabilisation and the pose estimation of UAVs. Some implementations of these stabilisation algorithms make use of specialised cameras that "can be used to refocus at certain depths" (Bills *et al.*, 2011). This will allow the drone to maintain a certain distance from specific visual elements. The study by Moore et al. (2009) made use of this concept where two UAV mounted cameras are used to obtain stereo information on the UAV's height above the ground and the distance to potential objects (Moore *et al.*, 2009). This camera-mirror system uses specially shaped reflective surfaces that are associated with each camera to "map out a collision-free cylinder through which the aircraft can pass without encountering objects" (Moore *et al.*, 2009). This method of vision control is particularly effective for terrain following and object avoidance. The study by Johnson (2008) used vision based algorithms to make a quadrotor hover with attitude stabilization and position control using "first principles and a proportional-derivative control method" (Johnson, 2008). Additional studies that address the issue of stabilisation of a quadrotor include Kendoul et al. (2009) and Cherian et al. (2009) (Kendoul *et al.*, 2009) (Cherian *et al.*, 2009). Kendoul et al. (2009) make use of a low-resolution on board camera and an Inertial Measurement Unit (IMU) to estimate optic flow, UAV motion and depth mapping. Cherian et al. (2009) proposed a new algorithm to estimate UAV altitude by using images taken from the downward facing camera of the UAV (Cherian *et al.*, 2009). This algorithm would use texture information of the image from the downward facing camera and to determine the altitude of the UAV.

### 2.5.8 Navigation patterns

In the study by Tournier et al. (2006), vision based navigation is investigated by using known patterns and environments (Tournier *et al.*, 2006). These patterns and environments are represented using large image databases of the environment. Moire patterns were pasted into the environment the UAV was navigating to estimate the position and altitude of the quadrotor. Courbon et al. (2009) and Soundararaj et al. (2009) used vision to navigate known environments (Courbon *et al.*, 2009) (Soundararaj *et al.*, 2009). However the methods that were used in these studies are not applicable to scenarios where a large image database of the environment is not available. The study by Mori et al. (2007) used markers to facilitate navigation between two markers (Mori *et al.*, 2007) (Bills *et al.*, 2011).

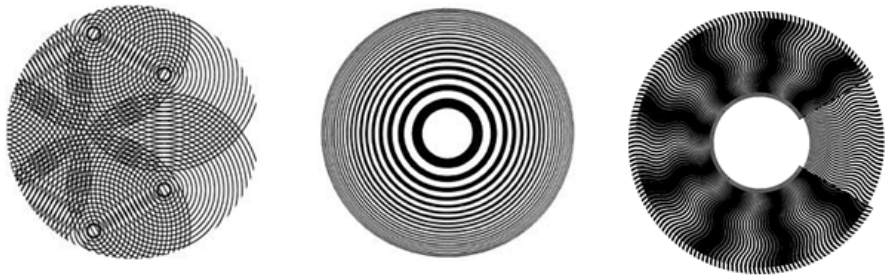

Figure 2.7: Moire patterns

#### Summary

The related work discussed illustrates the various methods that can be used to implement flight automation. A specific set of sensors is required to implement each method. The AR Drone supports the required sensors to perform visual based navigation and therefore a system will be implemented to perform detection, recognition and tracking using the drone's available sensors.

## 2.6 Conclusion

The literature discussed shows that there are many types of drones with varying capabilities. The hardware and software components of a drone determine various functions that a drone can perform. It also shows that there are many methods that can be used to implement a flight navigation system. Each method requires the use of a specific set of sensors and algorithms, depending on the desired function of the drone. A brief overview of existing drone applications is provided to illustrate some

drone capabilities. This serves to indicate the differences, advantages and disadvantages of drones and their applications. This background information served as a basis upon which a drone was chosen to implement a detection, recognition and tracking system. It also helped in choosing the tools and algorithms that are used to implement this system.

# Chapter 3

# Application Programming Interfaces (APIs)

## Introduction

To create a system to perform target detection, recognition and tracking various software development environments and tools need to be considered. Existing code libraries and integrated development environments will assist with the programming of, and interfacing with, the drone. The following sections describe the various APIs that were explored to determine which was best suited to carry out target recognition and tracking. This chapter will look at the Parrot AR Drone Software Development Kit (SDK) 2.0.1, EZ-Builder (EZ-B) generic robotics SDK and the AC Drone.

## 3.1 Parrot AR Drone SDK 2.0.1

The AR Drone has an open source API that is widely used as a research standard for developing AR Drone applications. The API available at (AR.Drone, 2009) includes a software development kit (SDK) that has been written in C and runs on iOS, Android and Linux platforms. The API does not however give the developer access to software that is embedded on the drone. There are four components, also called communication services that are implemented in the SDK. These components provide information on the state of the drone and allow the user to control and configure the drone. These communication services are AT Commands, Navigation Data, video stream and the control port.

## 3.2 AT Commands

AT commands are used to send commands and configuration requests to the AR Drone. The command syntax is as follows:

**"AT*PCMD=<sequence_number>,<flag>,<roll_p>,<pitch_p>,<gaz_p>,<rot_p>"**

Sequence number refers to the command's turn for execution. This number depends on the number of commands that have come before it (Portal, 2011). The flag argument defines whether the drone will look at the arguments that follow it. When the flag is 1 (True) the AR Drone will look at the arguments roll, pitch, gaz and rotation. When the flag is set to 0 (False), the drone will perform the "hover" command and attempt to maintain the same position using algorithms to cancel the inertial speed of the drone. Each argument is explained below. Refer to Figure 2.3 for an illustration of the movement direction.

### 3.2.1 Roll argument

The argument roll_p is a double value that can be set in the range [-1..1]. This value represents a "percentage of the max value of the angle roll that the drone can achieve." (Portal, 2011) The maximum amount of roll that the drone can achieve is hard coded at 12 degrees. To illustrate this, if we set roll_p at 0.5 the AR Drone will shift 6 degrees in the roll angle which will cause the drone to move to the right. The drone will perform the opposite when roll_p is set to -0.5.

### 3.2.2 Pitch argument

The argument pitch_p is also double value that can be set in the range [-1..1]. This value represents a "percentage of the max value of the angle pitch that the drone can achieve." (Portal, 2011) The maximum amount of pitch that the drone can achieve is hard coded at 12 degrees. To illustrate this, if we set pitch_p at 0.5 the AR Drone will shift 6 degrees in the pitch angle which will cause the drone to move to the backwards. The drone will perform the opposite when pitch_p is set to -0.5.

### 3.2.3 Gaz argument

The argument gaz_p is also double value that can be set in the range [-1..1]. This value represents a "percentage of the max value of the vertical speed that the drone can achieve." (Portal, 2011) The

maximum vertical speed that the drone can achieve is hard coded at 0.7m/s. To illustrate this, if we set gaz_p at 0.5 the AR Drone will travel on the Z axis with a speed of 0.35m/s which is the upward movement of the drone. The drone will perform the opposite when gaz_p is set to -0.5.

### 3.2.4 Rotation argument

The argument rot_p is also double value that can be set in the range [-1..1]. This value represents a "percentage of the max value of the angular speed that the drone can achieve." (Portal, 2011) The maximum angular speed that the drone can achieve is set at a default of 100 degrees. To illustrate this, if we set rot_p at 0.5 the AR Drone will turn right at an angle of 50 degrees. The drone will perform the opposite when rot_p is set to -0.5.

### Summary

These commands make it easy for the user to control the drone. If the user wants the drone to hover, an AT Command with a flag value of 1 should be set and all the other arguments set to 0. The drone will produce a standard amount of lift and not move from its position but will slide a little due to inertia. The drone has a built in algorithm to cancel inertia that can be employed by sending an AT Command with just the flag value set to 0. The algorithm makes use of the downward facing camera to attempt to stay above the same spot. This is called the "hover" procedure (Portal, 2011). By setting values for the last four arguments the user can make the drone perform complex flight patterns for example the command:

**"AT*PCMB=<1>,<1>,<0.25>,<0.25>,<0.5>,<0.25>"** will make the drone roll 3 degrees to the right, go backwards at an angle of 3 degrees, rotate to the left and ascend at 0.35m\s.

## 3.3 Navigation Data

The Navigation Data communication service provides the API with all the information pertaining to the state of the drone such as the drone's altitude, speed and attitude. NavData also returns raw measurements taken from the Drones sensors. This NavData is sent to the client side API by the drone 200 times per second and 30 times a second when in demo mode.

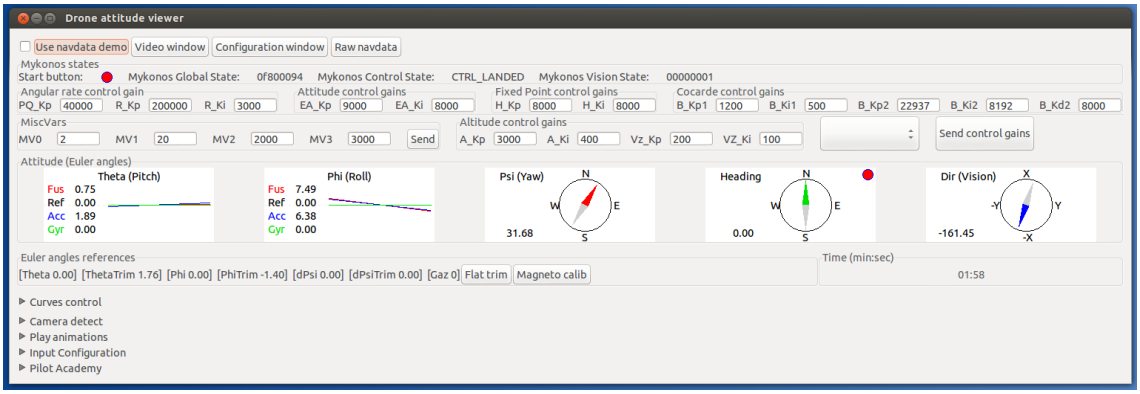


Figure 3.1: Navigation Data Interface (Stephane Piskorski, 2011)

## 3.4 Video Stream

The video stream communication service sends the video stream from the AR Drone to the client side application. The codecs that are included in the SDK are used to encode and decode the images of this video stream.

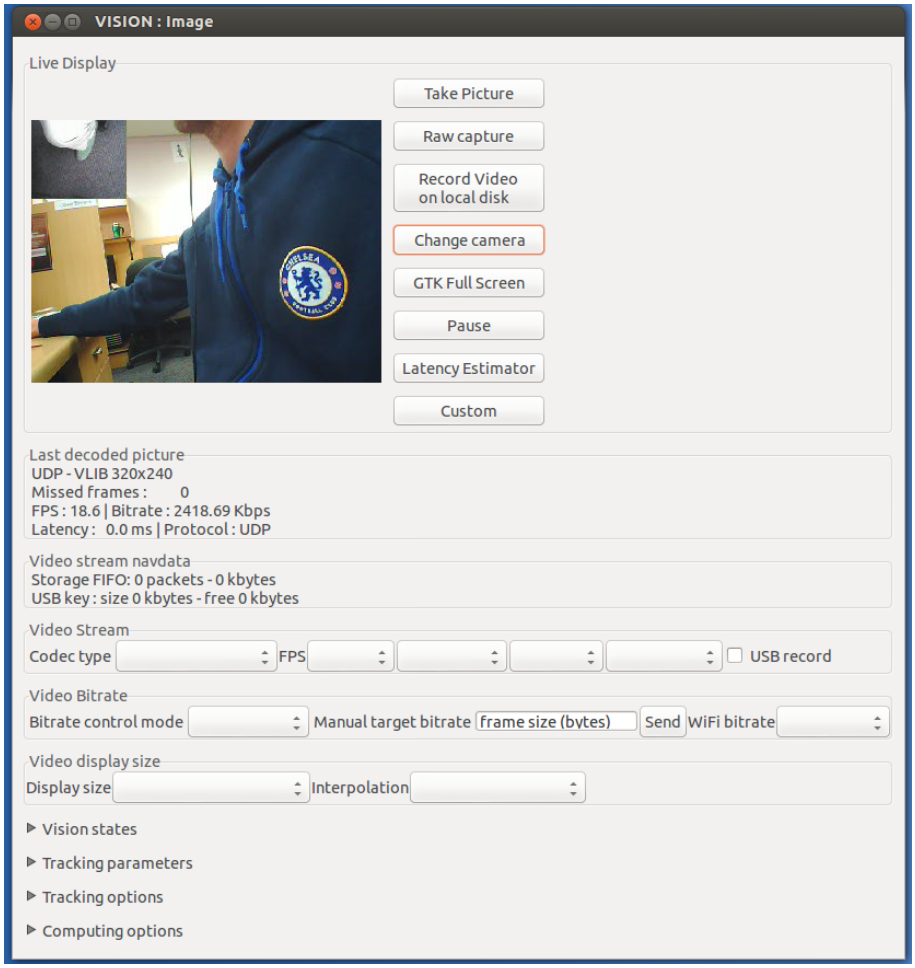


Figure 3.2: Parrot SDK Video Interface

## 3.5 The Control Port

The control port is a channel that is used to communicate critical data. It has been made to use a TCP connection so that data transfer is reliable. This channel is used in the configuration of the AR Drone when retrieving configuration data. It is also used to "acknowledge important information such as the sending of configuration information." (Dijkshoorn, 2012)

## 3.6 EZ-Builder Generic Robotics SDK

EZ-Builder (EZ-B) (Sures, n.d.) is a generic robotics software development kit created by Canadian Roboticist DJ Sures that allows developers to interface with various types of robots. The robot

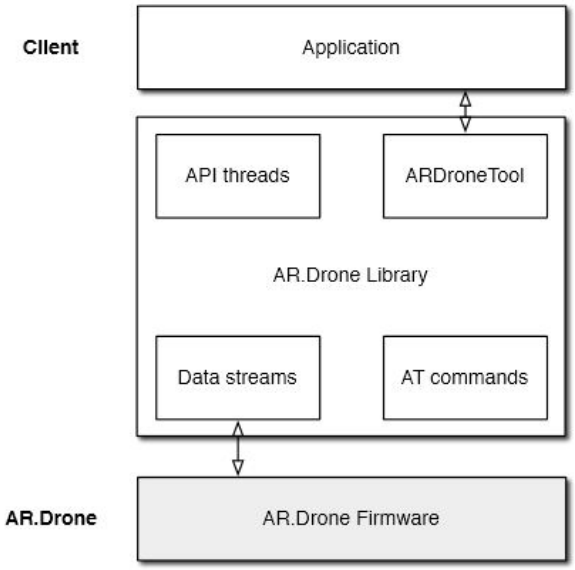


Figure 3.3: Layered architecture of a client application built upon the Parrot AR Drone SDK (Dijkshoorn, 2012)

control software has a GUI interface as well as a C#, VB and C++ programming environment. Using EZ-B, various tracking algorithms were implemented by exporting the video feed to OpenCV for image processing. This processed image was then sent back to EZ-B for the execution of various tracking directives and scripts such as velocity tracking and search algorithms.

### 3.6.1 Video Interface

The EZ-B initiates a link to the AR Drones video stream. This stream can then be affected using OpenCV functions to enhance the quality of the image. Image brightness, contrast and saturation can be adjusted from this interface. The pixel density of the stream can also be swapped between 640x480 and 320x240. This interface also allows one to record the video stream to file.

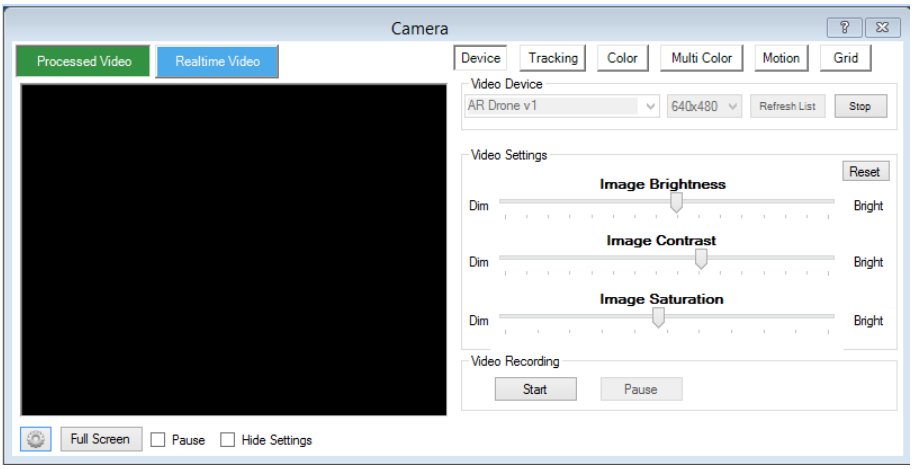


Figure 3.4: EZ-Builder Video Interface

### 3.6.2 Script Manager

The EZ-B allows one to create scripts that can be executed at various points of flight execution such as the detection of faces, glyphs and QR codes. EZ-B uses its own programming syntax which give the developer access to various robot functions. The script manager also provides a debugging interface and a live variable watch table so that flight and program data can be monitored during tests.

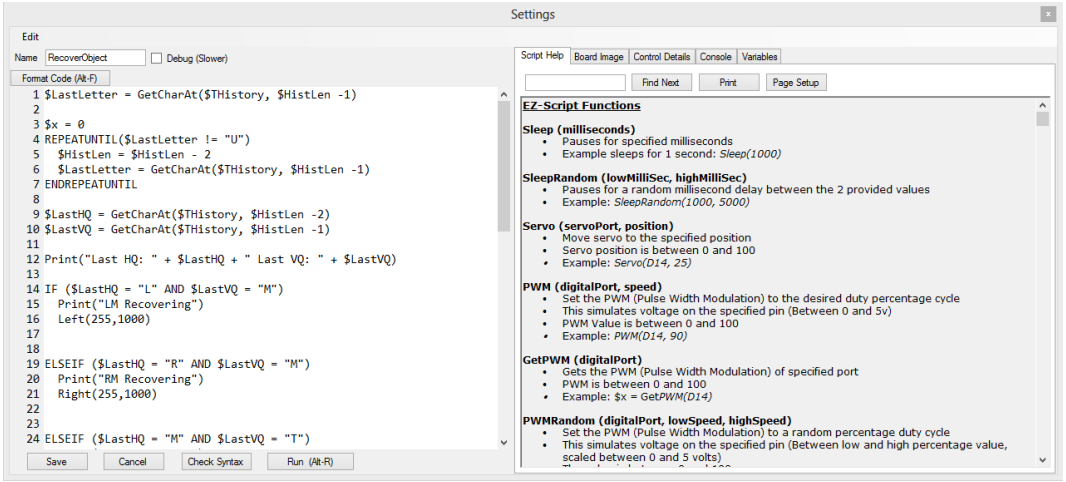


Figure 3.5: Script Manager Interface

## 3.7 CV Drone

CV Drone (puku0x, 2012) is a C++ library created by a Japanese developer that goes by the name of puku0x. This open source library uses OpenCV 2.4.6, FFmpeg 2.0 and POSIX Threads for AR Drone development (puku0x, 2012). The library allows the developer to take control of navigation data and the video stream for the development of any PC based application. The roll, pitch, yaw and altitude velocities can be set by setting these respective variables. The library also provides access to flight animations that are pre-programmed onto the drone such as LED control and flight animations. Examples of these animations are for the LEDs to blink a specific colour or for the drone to rotate a specific number of degrees.

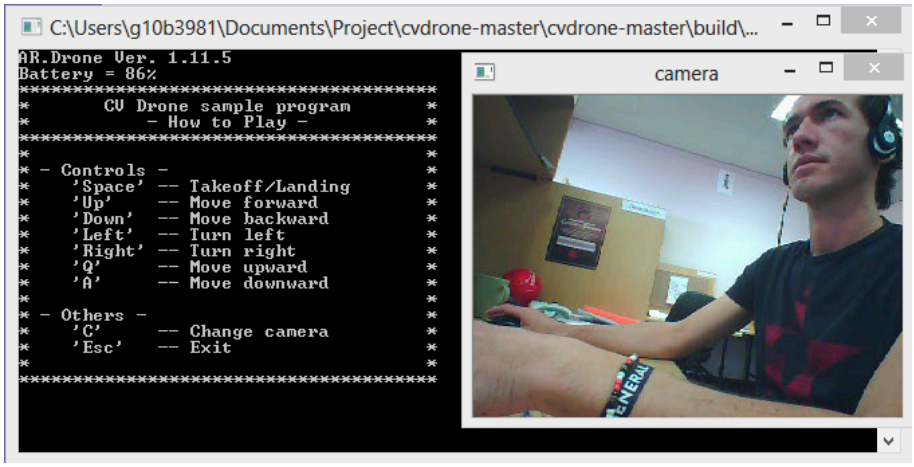


Figure 3.6: ACDrone Main Interface

Figure 3.6 illustrates the custom command interface in which the drone is controlled. A simple video feed is also displayed using OpenCV.

## 3.8 Conclusion

The various API's discussed show the different ways in which on can interface with the AR Drone. Each API has a set of tools and programming facilities that can be used to implement a detection, recognition and tracking system. Investigating the strengths and weaknesses of each API provided insight into the capabilities of the AR Drone as well as the methods that can be used to create. This information helped in selecting the most appropriate API to implement each algorithm used in the system.

# Chapter 4

# Design and Tools

This chapter describes the software tools and algorithms used to perform detection, tracking and recognition functions.

## 4.1 OpenCV

OpenCV is an open source computer vision software and machine learning software library that was selected to execute the various tracking and recognition algorithms. OpenCV contains a library of several hundred algorithms that can implement computer vision and image processing. The computer vision algorithms are aimed at performing real-time image processing and are optimised to cope with these requirements. The algorithms in the OpenCV library can be used to identify objects, classify human actions in videos, track camera movements, detect faces and extract 3D models of objects to name a few (OpenCV, 2013b).

OpenCV was chosen for this research over other image processing libraries such as MATLAB for various reasons. OpenCV is written in C/C++ which provides fast algorithm execution speeds as C/C++ is closer to machine language than languages like Java. This minimises that amount of code interpretation that needs to be performed leaving more processing cycles for image processing. OpenCV only requires approximately 70Mb of RAM to run in real-time. OpenCV is open source, extensively supported and is portable across Windows, Linux and MacOS. The full documentation on OpenCV can be found online (OpenCV, 2013b).

## 4.2 CamShift algorithm

CamShift stands for Continuously Adaptive Mean Shift as this algorithm is based on the Mean Shift algorithm. CamShift is commonly used as an object tracking tool and is used as one method of tracking objects and faces in OpenCV. It combines the Mean Shift algorithm with an adaptive region-sizing step. CamShift is able to handle dynamic distributions as it can adjust its search window size for the next image frame based on the zeroth moment of the current frames distribution (Isaac Gerg, 2003).

### Mean Shift Algorithm

The mean-shift algorithm is technique used to locate the maxima of a probability density function which is useful for finding the centroid of a coloured object (Belisarius, 2011) and hence the object itself. To illustrate this consider a set of points representing a pixel distribution. A small window can be drawn onto this pixel distribution and the goal of the algorithm is to move the window to the area of maximum pixel density. Figure 4.1 shows the first window in blue and is labeled as "C1". The circles center is marker with a blue rectangle named "C!_o". By finding the centroid of all the points in the window "C1" we get point "C1-r" drawn as a small blue circle. This is the real centroid of the blue window. The window now needs to be moved so the the so that the new point "C1-r" is the centre of the window. This process is performed over and over until a window is obtained that contains the maximum pixel distribution.

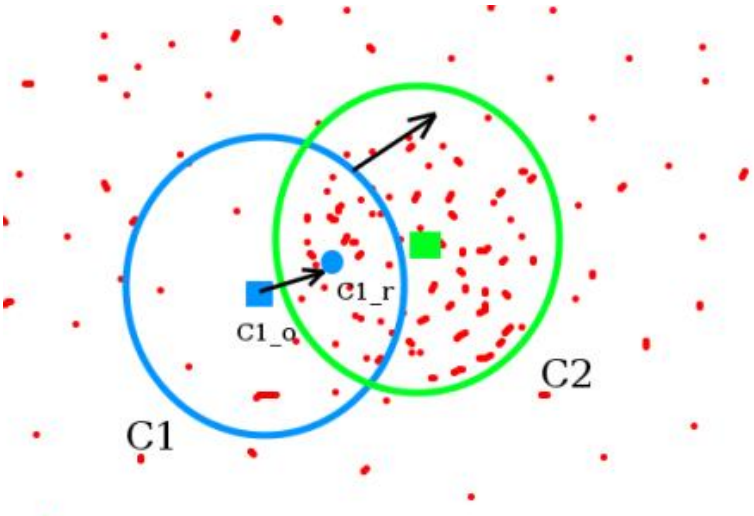


Figure 4.1: Meanshift Maximum Pixel Density (OpenCV, 2013b)

The Mean Shift algorithm uses three inputs to determine the centroid of the object. A measurement of distance between pixels, radius within which all pixels will be effected by the maxima and a value difference. This will determine which pixel values are used to calculate the mean. Figure 4.2 illustrates how the centroid of each object is calculated and used to shade that object to its maxima value.

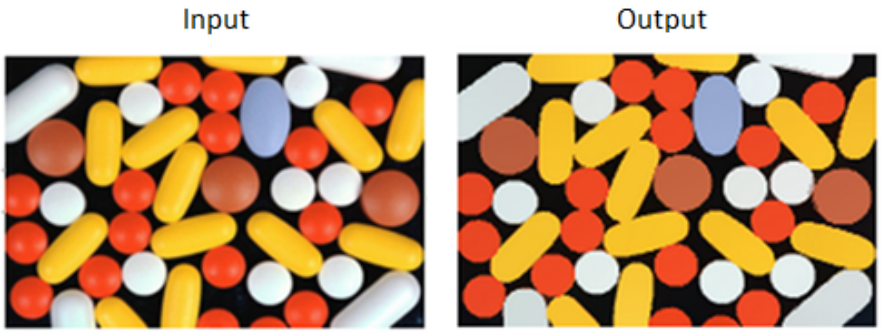


Figure 4.2: Mean Shift Filter (Belisarius, 2011)

### CamShift Algorithm

The CamShift algorithm differs from the Mean Shift algorithm as it uses continuously adaptive probability distributions rather than a static distribution. This difference allows the CamShift to recompute distributions for each frame which makes it useful in video as this allows the algorithm to anticipate object movement to quickly track an object between frames. The makes CamShift effective in tracking objects moving quickly.

The standard steps of the CamShift algorithm are as follows:

1. Select the location in the search window that is to be tracked. This is the Mean Shift search window. This sets the hue of the object that is going to be tracked. This hue can also be set using a colour wheel or a similar colour selection method.

2. Calculate the probability distribution of the selected area centred at the Mean Shift window. This is represented as a histogram of colours which represents the object. The height of each bar on the histogram represents the amount of pixels that have that hue in the selected region.

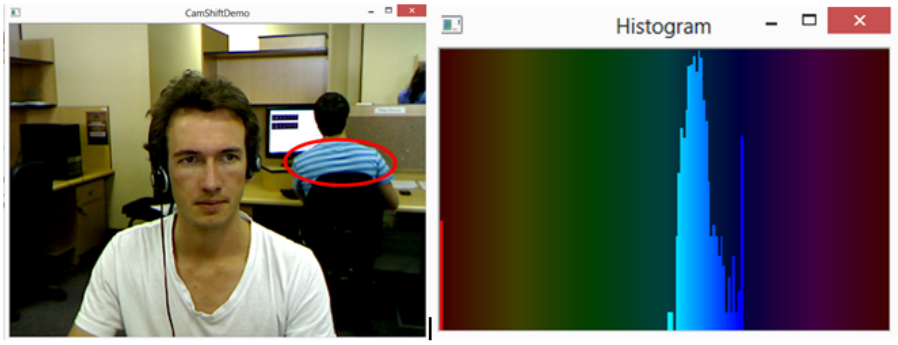


Figure 4.3: CamShift Histogram

3. Iterate the Mean Shift to find the maxima/centroid of the probability image. Use this point as the zeroth moment. This will be the new centre point of the search window.

4. For all following frames, centre the search window at the new centroid and repeat from Step 2. (Allen *et al.*, 2004)

## Centroid Calculation

The centroid calculation in Step 2 is found using moments (Bradski, 1998). Given that I(x,y) is the intensity of the discrete probability image at (x,y) within the search window. The zeroth moment is found using:

$$M_{00} = \sum_x \sum_y I(x,y)$$

The first moment for x and y is then found using:

$$M_{10} = \sum_x \sum_y xI(x,y)$$

$$M_{01} = \sum_x \sum_y yI(x,y)$$

The mean search window location is then computed using:

$$x_c = \frac{M_{10}}{M_{00}};\ y_c = \frac{M_{01}}{M_{00}}$$

Certain problems have been identified when using centroid computation for face tracking (Bradski, 1998). The projection of the distribution histogram onto consecutive frames has been known to

introduce a bias in the target location estimate (Allen *et al.*, 2004).

### Glyph Recognition

Once a glyph has been found it can be extracted from the main image using Quadrilateral Transformation. This transforms any quadrilateral from an image into a rectangular image. Many glyph images that are detected will be at various angles and depths and so quadrilateral transformation serves to standardise the image to be input to the glyph recognition algorithm.

Using the transformed glyph image we can perform glyph recognition. This can be performed in various ways such as shape recognition or template matching. As the glyph is divided up into rows and columns when it is constructed, these rows and columns can be remapped to the transformed image to determine individual cell colours. After remapping the cells to the image, every white and black pixel in the cell can be counted to determine to original colour of the cell. Whichever colour occurs most in each cell can be assumed to be the original colour of the entire cell. The ratio of black to white pixels will also indicate a degree of certainty that can be used further when comparing the glyph to known glyphs. The glyphs resulting colour can then be mapped to a matrix of 1's and 0's that represent black and white respectively. This matrix can be used to match the glyph against know glyph matrices. Known glyphs are stored in their binary matrix representation. Each black square of the glyph represented as a 0 and each white square represented as a 1 as can be seen in Figure 4.11. It is highly likely that a detected glyph may have been rotated in the image or by quadrilateral transformation. This would cause the glyphs matrix representation to be different when reconstructed. This problem can solved by either storing all four matrix representations for one glyph or by rotating the reconstructed glyph matrix. This matching process requires glyphs to maintain a unique matrix representation for each rotation.

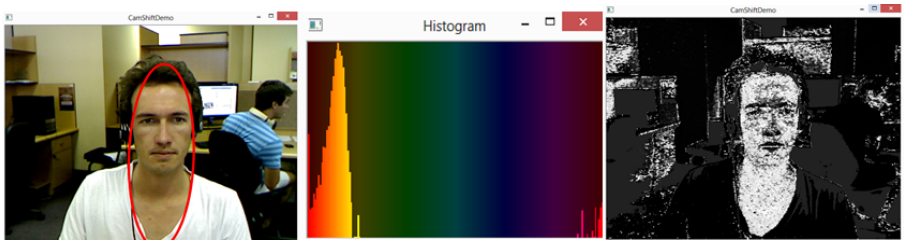


Figure 4.4: CamShift backprojection

## 4.3 Viola Jones

Viola Jones is a "machine learning approach for visual object detection which is capable of processing images extremely rapidly and achieving high detection rates" (Viola *et al.*, 2005). This section will focus on Viola and Jones's contribution to object detection in the context of face detection. Their contribution came in three parts.

1. Creation of a classifier that was based upon a combination of weaker classifiers using the AdaBoost machine learning algorithm (Viola *et al.*, 2005). These weak classifiers represented very simple features used to detect a face.

2. Viola and Jones created their own implementation of a standard algorithm to combine classifiers to create new classifiers. Although their algorithm could take time to detect a face, it's strength was in its ability to rapidly reject regions of an image that did not contain a face.

3. Viola and Jones used a new image representation called an integral image (Viola *et al.*, 2005) that could effectively pre-compute most costly operations that were needed to execute their classifier at once (de Souza, 2012).

### Classifier Selection

The classifiers that Viola and Jones use are Haar-like features. These features each represent the differences in grey scale intensity between numerous adjacent rectangular areas in an image. These classifiers detect an object by summing the pixel in dark side of classifier and the light side. The difference in these values determines if there is a match. These Haar-like features are effective owing to the uniformity of shadow distribution on the human face. Figure 4.5 illustrates the feature matching of the Haar-like features:

Figure 4.5: Feature Matching Using Haar-like Classifiers (de Souza, 2012)

## Classifier Matching

The algorithm to search for a feature match in an image starts by creating a search window on the image. This section on the image is then searched exhaustively for classifier matches. On completion of the search, the search window is adjusted to a different part of the image and repeats the search process. The search window will have traversed the entire image by the time scanning is complete. Classifier matching efficiently discards search windows that have unpromising results. In search windows that weakly match a classifier, more time is spent trying to check that other classifiers will not match. When the algorithm eventually cannot reject a search window it concludes that it contains a face.

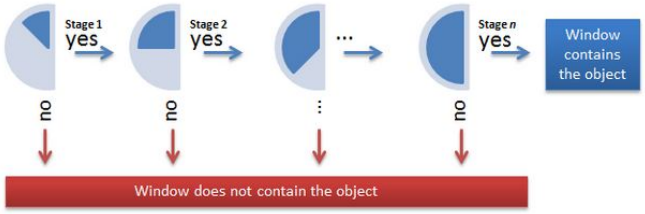


Figure 4.6: Weak Classifier Cascade (de Souza, 2012)

Matching uses a cascading technique to combine classifiers in such a way that a classifier is only processed when its preceding classifiers have successfully matched. The classification scheme used by Viola Jones is a cascade of boosted classifiers. Meaning that each stage of the cascade is a stronger classifier owing to the combined positive matches of previous stages. Each weak classifier has a high probability of successfully being matched to an image. This alone is nowhere near enough proof to assume a face is present but a combination of many of these weak classifiers increases the probability of a match being made. Figure 4.6 illustrates how weak classifiers are cascaded through to detect a face or object.

## Integral image representation

Thus far the Viola Jones algorithm is effective in quickly discarding search windows with no matches. However, the algorithm needs to perform matching over several scaled regions on the image to complete a scan and this can be time consuming (de Souza, 2012). To alleviate this problem, Viola and Jones introduced the integral image representation. This was done by caching the sums of rectangles for every feature instead of recomputing the value after every rescaling of the search

window. This was done by creating a summed area table for the frame being processed by computing all possible rectangular areas in the image. This saves time as it can be computed in a single pass over the image using the recurrence formula shown in Figure 4.7. Looking at the integral image representation in Figure 4.7 one can see that the top left value is the same value as original image. The values adjacent to the top left value of the integral image are then calculated as the sum of the original images values at this point and any previously calculated adjacent values. The value 13 in the integral image is the sum of its adjacent values 7 and 6. These calculations are performed throughout the image.

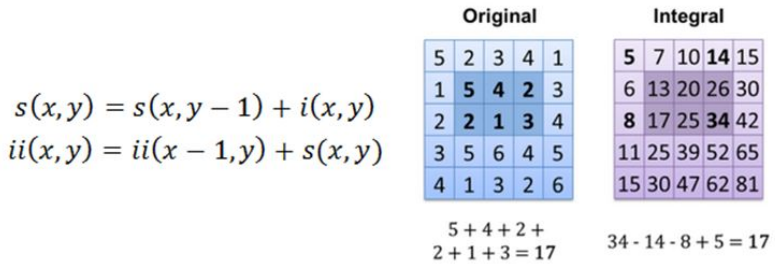


Figure 4.7: Recurrence Formula and Integral Image Example (de Souza, 2012)

## 4.4 Fiducial Marker/Glyph Recognition

Fiducial markers, also known as Glyphs, are 2D images of a square grid that is divided into rows and columns. Each cell on the grid is either given a black or white colour. The outer most edge of the grid is all black giving the glyph a boarder. Each row and column has to have at least one white cell so that the boarder of the glyph can be easily identified.

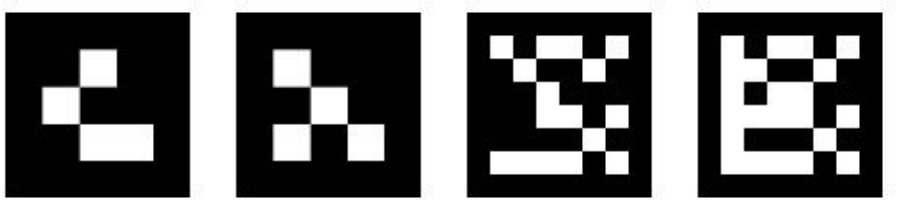

Figure 4.8: Glyph Samples (Kirillov, 2010)

The most popular use of glyphs has been in the field of augmented reality where a glyph is detected in a video stream and then substituted with an artificially generated object. This allows users to combine reality with virtual elements. Owing to the nature of glyphs, they have also been used to

provide instructions to robots such as navigation commands as each individual glyph can be easily told apart.

### Finding potential glyphs

Before glyphs can be told apart, the image feed needs to be analysed to search for potential glyphs. This task involves finding all quadrilateral areas that bear the attributes of a glyph. Finding the four corners of the glyph serves as a mechanism to locate glyphs. This can be performed using various image processing techniques such as grey scaling and thresholding. Grey scaling the image is the first logical step as colour is not needed to recognise glyphs. Grey scaling reduces the size of an images representation and removes the unnecessary noise of colour from the image. Grey scaling can be performed in various ways but most methods use percentages of an images red, green and blue (RGB) pixel values to calculate a single grey scale value for that pixel. An example of this calculation is as follows:

**Gray = 0.299 x Red + 0.587 x Green + 0.114 x Blue**

To further isolate the glyphs a custom threshold must be applied to image taking into account the various lighting conditions of the image. A particularly effective thresholding technique for this is Otsu's thresholding method.

### Otsu's Thresholding Method

Otsu's thresholding method iterates through every possible thresholding value and uses the results to calculate the optimal measure of spread of pixels either side of the threshold. This determines which threshold value renders and image where the sum of foreground and background spreads is at a minimum. This effectively splits pixels into foreground or background pixels. Figure 4.10 illustrates the optimal split of pixels according to their calculated variances. The graphs in Figure 4.10 illustrate the number of pixels of each value in the image. A pixel value is then calculated to determine where the split between background pixels and foreground pixels should occur. The respective background and foreground pixels are illustrated in the graphs in the right part of Figure 4.9.

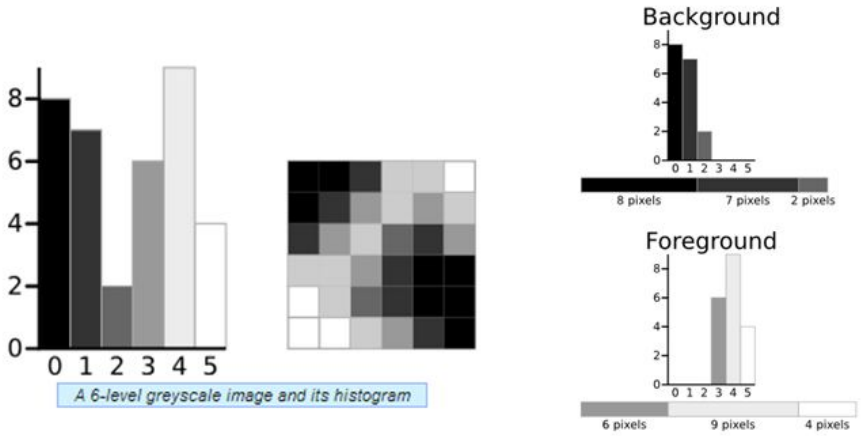


Figure 4.9: Otsu Thresholding: Foreground and Background (Greensted, 2010)

The next step is to calculate 'Within-Class Variance' which is a sum of the weighted variance between the foreground and background. This 'Within-Class Variance' determines which threshold value we use. The result of Otsu's thresholding applied on glyphs is illustrated in Figure 4.10.

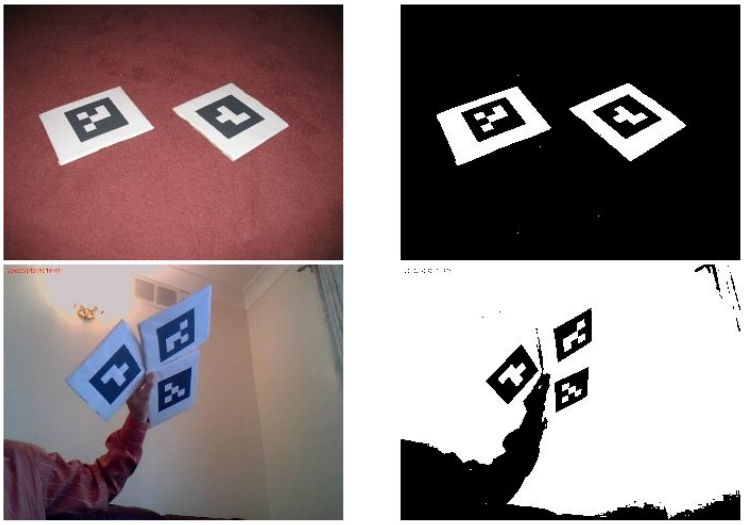

Figure 4.10: Otsu's Thresholding Results (Greensted, 2010)

Otsu's thresholding becomes problematic when dealing with images in environments whose illumination conditions vary regularly. A method that deals effectively with illumination variances is difference edge detection.

### Glyph Recognition

Once a glyph has been found it can be extracted from the main image using Quadrilateral Transformation. This transforms any quadrilateral from an image into a rectangular image. Many glyph images that are detected will be at various angles and depths and so quadrilateral transformation serves to standardise the image to be input to the glyph recognition algorithm.

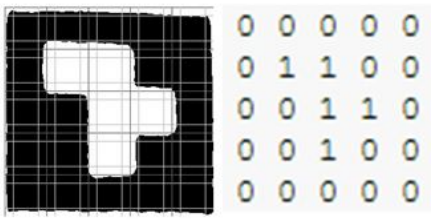


Figure 4.11: Glyph Grid Remapping (Kirillov, 2010)

Using the transformed glyph image we can perform glyph recognition. This can be performed in various ways such as shape recognition or template matching. As the glyph is divided up into rows and columns when it is constructed, these rows and columns can be remapped to the transformed image to determine individual cell colours. After remapping the cells to the image, every white and black pixel in the cell can be counted to determine to original colour of the cell. Whichever colour occurs most in each cell can be assumed to be the original colour of the entire cell. The ratio of black to white pixels will also indicate a degree of certainty that can be used further when comparing the detected glyph to known glyphs. The glyphs resulting colour can then be mapped to a matrix of 1's and 0's that represent black and white respectively. This matrix can be used to match the glyph against know glyph matrices. Known glyphs are stored in their binary matrix representation. Each black square of the glyph represented as a 0 and each white square represented as a 1 as can be seen in Figure 4.11. It is highly likely that a detected glyph may have been rotated in the image or by quadrilateral transformation. This would cause the glyphs matrix representation to be different when reconstructed. This problem can solved by either storing all four matrix representations for one glyph or by rotating the reconstructed glyph matrix. This matching process requires glyphs to maintain a unique matrix representation for each rotation.

## 4.5 Face Recognition

This section will cover two face recognition algorithms. The Eigenfaces algorithm and the Fisherfaces algorithm. Face detection and face recognition are two different concepts. Face detection discerns a human form by focusing on facial features that are common across all faces. Face detection can be used to determine the race, gender or ethnic origin of a face but cannot obtain a positive identification of the owner of the face. Face recognition focuses on making a positive identification of the face by cross referencing the face with a database of faces. The key to face recognition is determining a confidence factor on the face being matched against to avoid returning false positives.

### 4.5.1 Eigenfaces

The Eigenfaces face detection algorithm uses Principal Component Analysis and distance based mapping to recognise a face. Recognition is performed by comparing an unknown face to a sample set of face images. These images contain various images of the faces to be matched. Recognition is performed using the following steps:

1. Calculate the "distance" between the unknown face and the sample set of faces.
2. Choose the sample image that is the closest match to the unknown image. This image has the highest probability of being a match to the unknown face.
3. If the "distance" to the sample image clears a certain threshold, the unknown image is determined as recognised. If the "distance" is below the threshold, the new face is classified as unknown (Turk & Pentland, 1991).

#### The "Distance" Between Images

The "distance" between images refers to the Euclidean distance between the images. In a 3D space this is computed as:

$$\text{sqrt}(dx^2 + dy^2 + dz^2)$$

Eigenfaces takes into account the dimensions of a face image by considering pixel locations as a separate dimension. This is utilised using a dimensionality reduction method, namely Principal Component Analysis (PCA). PCA allows one to represent multiple dimensions of information in fewer dimensions. For example, if one was planning a trip across a map, the 2D locations of various

destinations could be represented using a 1D line that connects the locations. This reduction in dimensionality is illustrate in Figure 4.12.

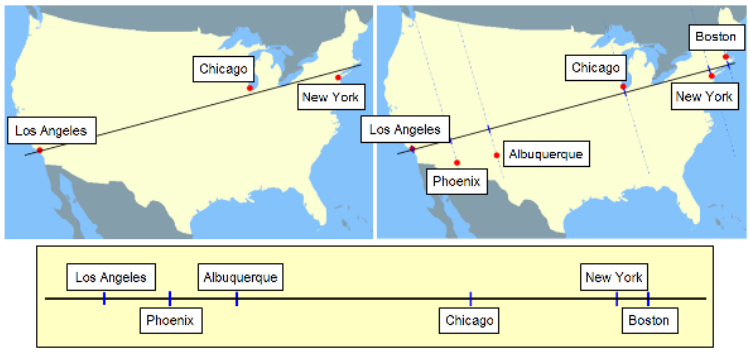


Figure 4.12: Dimensionality Reduction Using PCA (Hewitt, 2007)

As can be seen from Figure 4.12 the lines do not perfectly match up. This is the error or "noise" created when reducing dimensionality. This error is minimised by calculating a line between the points that has the smallest distance of deviation between the line and the locations. Now that an image can be represented in a lower dimension, the 2D points in the image need to be represented as 1D points. This is performed using projection. Projection takes a 2D point and allocates it to a subspace location that is as close to the higher dimension as possible. The blue marks on the 1D line that mark the location of cities are the projected points and the line itself is the subspace (Hewitt, 2007).

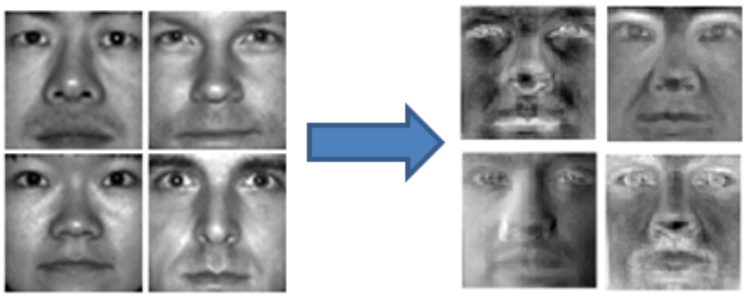

Figure 4.13: Face Images Mapped to Eigenfaces (Hewitt, 2007)

In summary, Eigenfaces determines the distance between an unknown image and the sample set of images by measuring the "distance between their points in a PCA subspace (Hewitt, 2007)." If sample images with 50x50 pixel dimensions are being used, the subspaces allows us to compare

images in a simplified PCA subspace rather than the 2,500 dimensional image space. The image's 2,500 dimensions can be used to define the slope of a line for each image. This line is then used to create an image that represents the Eigenvector by placing each value in its corresponding pixel location. The produces face like images also known as Eigenfaces.

### 4.5.2 Fisherfaces

Fisherfaces is a similar face recognition algorithm that uses dimensionality reduction to recognise faces. Fisherfaces uses Linear Discriminant Analysis (LDA) to find the subspace within which a set a sample face images can be represented. The vectors that define these subspaces are known as Fisherfaces (Belhumeur *et al.*, 1997). The Fisherfaces algorithm is more robust than Eigenfaces as it is insensitive to lighting variations and facial expressions.

#### Linear Discriminant Analysis

LDA is an enhancement to PCA as PCA does not use class information. PCA scatter matricies are effective in reconstructing an image from a low dimensional basis but they are not effective from a discrimination point of view. LDA creates "a discriminant subspace that minimizes the scatter between images of the same class and maximizes the scatter between different class images (Hwang *et al.*, 2004)." Fishers's Linear Discriminant (FLD) attempts to arrange the scatter graph in a way such that classification is more reliable (Belhumeur *et al.*, 1997).

Fisherfaces defines the between-class scatter matrix as:

$$S_B = \sum_{i=1}^{c} N_i(\boldsymbol{\mu}_i - \boldsymbol{\mu})(\boldsymbol{\mu}_i - \boldsymbol{\mu})^T$$

and the within-class scatter matrix as:

$$S_W = \sum_{i=1}^{c} \sum_{\mathbf{x}_k \in X_i} (\mathbf{x}_k - \boldsymbol{\mu}_i)(\mathbf{x}_k - \boldsymbol{\mu}_i)^T$$

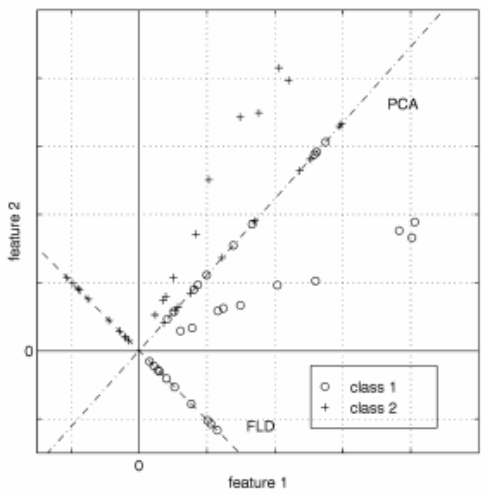


Figure 4.14: Discrimination of Class Information

The Figure 4.14 illustrates the benefits of class specific linear projection. It compares PCA and FLD for a two-class problem where the samples used for each class are randomly altered form its normal state in a direction perpendicular to a linear subspace.

## Algorithm Description

Let X be a random vector with samples drawn from c classes:

$$X = \{X_1, X_2, \ldots, X_c\}$$
$$X_i = \{x_1, x_2, \ldots, x_n\}$$

The scatter matrices S_{B} and S_{W} are calculated as:

$$S_B = \sum_{i=1}^{c} N_i(\mu_i - \mu)(\mu_i - \mu)^T$$
$$S_W = \sum_{i=1}^{c} \sum_{x_j \in X_i} (x_j - \mu_i)(x_j - \mu_i)^T$$

where $\mu$ is the total mean:

$$\mu = \frac{1}{N} \sum_{i=1}^{N} x_i$$

And μ{i} is the mean of class i ∈ {1,...,c}:

$$\mu_i = \frac{1}{|X_i|} \sum_{x_j \in X_i} x_j$$

Fisher's classic algorithm now looks for a projection W, that maximizes the class separability criterion:

$$W_{opt} = \arg\max_W \frac{|W^T S_B W|}{|W^T S_W W|}$$

According to Belhumeur et al. (1997), a solution for this optimisation problem is given by solving the General Eigenvalue Problem:

$$\begin{aligned} S_B v_i &= \lambda_i S_w v_i \\ S_W^{-1} S_B v_i &= \lambda_i v_i \end{aligned}$$

# Chapter 5

# Implementation

## 5.1 Introduction

The following chapter deals with the implementation of various tracking algorithms. The implementation was performed across a range of mediums including C++, python and EZ-B. Implementation began with the goal of determining whether a quadrotor is a feasible medium to execute detection, recognition and tracking. To test this, various methods of detection and tracking were implemented. The following sections will cover the implementation of CamShift tacking, Haar-Cascade tracking, fiducial marker/glyph recognition and the tracking implementation. Many of the algorithms make use of OpenCV. The version that has been used in these implementations is version 2.4.6.

## 5.2 Connecting to the AR Drone

To connect to the AR Drone, the Parrot SDK 2.0 was used. The drone uses a Wi-Fi connection to connect to a client program. The AR Drone can be controlled by any device that can support a Wi-Fi connection. The connection process is as follows:

1. When the drone is powered up it creates a Wi-Fi network with the default ESSID of the format ardrone_xxx where xxx is a random sequence of numbers. The drone then allocates itself an odd IP address on the network (most commonly 192.168.1.1).
2. The user then connects a client device to the networked. This can be a smart phone or PC.
3. As the drone is acting as the server, the client device requests an IP address from the drones DHCP server.

4. The drone's DHCP server then allocates the client program an IP address. This IP address is the drone's IP address plus a random number between 1 and 4.

5. The client device can start sending commands and requests to the AR Drone and start receiving data via service ports.

The Parrot AR Drone SDK 2.0 provides control of the drone using three main services. The flight control and configuration service, navigation data service, and the video stream service.

Controlling drone flight and configuration of the drone is performed by sending AT Commands as mentioned in Section 3.2. These AT Commands are sent through to the drone inside UDP packets on port 5556. AT Commands are regularly sent to the AR Drone. The drone receives approximately 30 AT Commands per second.

The navigation data service of the drone provides information about the state drone. This information includes the drones status, multi directional speed, orientation, engine rotation speed and altitude. This navigation data is sent to the AR Drone's client device in UDP packets over port 5554.

The video stream service is sent to the AR Drone's client in TCP packets on port 5555. The video codec the AR Drone uses is H264 (MPEG4.10 AVC). This is used to ensure high quality streaming and recording of the video stream. Certain parameters of the video stream can be customised. The number of frames per second (FPS) can be set up to 15 FPS. The bitrate can be set between 250kbps and 4Mbps and the resolution can be set to either 640x360 or 1280x720. This implementation sets the FPS at either 6 or 15 FPS and the resolution at either 320x240 or 640x360. The Ar Drone also outputs a video recording stream on request. This stream is sent to the AR Drone client in TCP packets on port 5553. The stream transmits H264-720p frames for recoding. This stream is disabled when the AR Drone client is not recording.

## 5.3 Setting up the CamShift algorithm

After connecting to the AR Drone an infinite loop is created to capture the video stream of the drone frame by frame. Each frame is captured as a pointer to an Ipl image for processing in OpenCV detailed in Listing 5.1:

```
// -------------------------------------------------------------------
// ARDrone::getImage()
// Description  : Get an image from the AR.Drone's camera.
// Return value : Pointer to an IplImage (OpenCV image)
```

```
//------------------------------------------------------------------------
IplImage* ARDrone::getImage(void) {
        // There is no image
        if (!img) return NULL;

        // Enable mutex lock
        if (mutexVideo) pthread_mutex_lock(mutexVideo);

        // Copy the frame to the IplImage
        memcpy(img->imageData, pFrameBGR->data[0], pCodecCtx->width *
                ((pCodecCtx->height == 368) ? 360 : pCodecCtx->height)
                * sizeof(uint8_t) * 3);

        // Disable mutex lock
        if (mutexVideo) pthread_mutex_unlock(mutexVideo);
        return img;
}
```

Listing 5.1: Capturing Video Stream Frames For Processing In OpenCV

This Ipl image is then converted to the Hue Saturation Value (HSV) colour space using the cvCvtcolor OpenCv method. This allows a specific HSV value to be set so that custom object colours can be tracked. To allow the user to set their own HSV values a window is created where the each of the HSV values can be customised to a specific colour. Once the HSV values are set, a binalized image is created from the original from so that a black and white image can be obtained of the object being tracked.

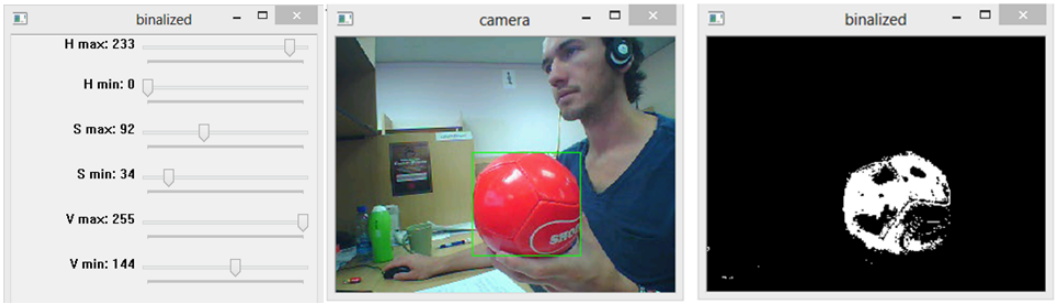


Figure 5.1: HSV Selection, Tracking Window and Binalized Image

This binary image is then cleaned up by performing opening and closing on the binalized HSV image. To further identify objects in the binary image a contour search is performed. This retrieves contours from the binary image and returns the number of contours retrieved. The largest of all the contours is then found. This contour will most likely be the object that is being searched for as it will be the largest object in the frame that matches the pre-set HSV values. A rectangle is then

created and placed around the object that is detected.

## 5.4 Tracking Implementation

Once the object has been detected in the video stream the quadrotor needs to make flight decisions based on the objects position. This was implemented by using the rectangle around the object to determine the centre point of the object. The processed video stream was then divided into nine quadrants. These quadrants are not all equally sized but rather slightly pushed to the edge of the video stream to create a larger quadrant in the centre. Figure 5.2 indicates the grid line positions.


Figure 5.2: Tracking Window Grid, Each Quadrant Number and Their Respective Flight Commands

Flight commands are then sent to the AR Drone according to which quadrant the centre of the tracked object falls into. In quadrant 4, the pitch of the AR Drone is set to move the drone forward. However, this forward motion cannot continue in definitely as the drone would crash in to the object it is tracking eventually. To prevent this, the program calculates the tracked objects total area (width x height) using the rectangle that was drawn around to object. If this area is under a certain threshold to drone executes the forward motion. Otherwise the drone holds its position a certain distance away from the object. A part of this tracking algorithm is detailed in Listing 5.2, then sets the value of one of four variables. These variables control the pitch, roll, altitude and yaw of the drone.

```
void trackObject(int quadrant, int obSize, double arr[]){
        double vx = 0.0, vy = 0.0, vz = 0.0, vr = 0.0;
        if(obSize > 200){ //this negates error of detection
                switch (quadrant){
                case 0:
                        printf("ascend + left \n");
                        vz =  1.0; //ascend
                        vr =  1.0; //left
                        break;
                case 1:
                        printf("ascend \n");
                        vz =  1.0; //ascend
                        break;
                case 2:
                        printf("ascend + right \n");
                        vz =  1.0; //ascend
                        vr = -1.0; //right
                        break;
                case 3:
                        printf("left \n");
                        vr =  1.0; //left
                        break;
                case 4:
                        if (obSize < 1500){ //so that it stays a certain
                                            distance away from the object
                        vx =  1.0;
                        printf("forward \n");
                        }
```

Listing 5.2: Object Tracking Options

These variables are calculated for every frame of the video stream before the move3D method is called. This method constructs the AT Command that will be sent to the AR Drone over Wi-Fi. It ensures that the drone is in flight before sending commands, increments the command sequence number and sets the mode of the PCMD command so that if all flight variables are zero, the drone can rest in hover mode. This allows the drone to execute various built-in algorithms that cancel inertial movement of the drone and assist the drone in maintaining a fixed position.

```
// ------------------------------------------------------------------------
// ARDrone::move3D(X velocity[m/s], Y velocity[m/s],
                   Z velocity[m/s], Rotational speed[rad/s])
// Description  : Move the AR.Drone in 3D space.
```

```
// Return value : NONE
// ----------------------------------------------------------------------------
void ARDrone::move3D(double vx, double vy, double vz, double vr) {
// AR.Drone is flying
        if (!onGround()) {
                // Command velocities
                float v[4] = {-vy*0.2, -vx*1.0, vz*0.1, -vr*0.5};
                int mode = (fabs(v[0]) > 0.0 || fabs(v[1]) > 0.0 ||
                                fabs(v[2]) > 0.0 || fabs(v[3]) > 0.0);
                // Limitation (-1.0 to +1.0)
                for (int i = 0; i < 4; i++) {
                        if (fabs(v[i]) > 1.0) v[i] /= fabs(v[i]);
                }
                // Send a command
                if(mutexCommand)pthread_mutex_lock(mutexCommand);
                sockCommand.sendf("AT*PCMD=%d,%d,%d,%d,%d,%d\r",
                        ++seq, mode, *(int*)(&v[0]), *(int*)(&v[1]),
                        *(int*)(&v[2]), *(int*)(&v[3]));
                if (mutexCommand) pthread_mutex_unlock(mutexCommand);
        }
}
```

Listing 5.3: AR Drone move3D Method

This algorithm created erratic flight in the AR Drone as it received numerous tacking commands every 30ms. This was overcome by sleeping the main method for 200ms to accommodate for motion delay. This helps to prevent the drone from executing a descend command 30ms after it started an ascend command. This also stops the occurance of "bounce" during flight. This could be caused by the drone executing, for example, an ascend command but instead of the object being centred within quadrant four the movement passes over quadrant four and straight into quadrant seven where a descend command will be sent immediately.

## 5.5 Setting up the various human feature tracking using Haar Cascades

In this section, the use of various Haar Cascades for tracking purposes is implemented. Each Haar Cascade uses OpenCV to track a human feature based on its specific classifier cascade. The cascades are constructed within XML files which contain various pieces of information about each classifier.

Each weak classifier feature contains the coordinates of the rectangles that need to be summed using the square matrix (the integral image), the dimensions of the rectangles and the weighting of the rectangle. It also contains a threshold value that determines whether the right_val or left_val is summed for the rest of the cascade. A single feature in the cascade is detailed in Listing 5.4 in XML.

```
<opencv_storage>
<haarcascade_upperbody type_id="opencv-haar-classifier">
        <size>22 18</size>
        .
        .
        .
        <!-- root node -->
        <feature>
                <rects>
                        <_>5 5 12 6 -1.</_>
                        <_>9 5 4 6 3.</_></rects>
                <tilted>0</tilted></feature>
        <threshold>-0.0136960297822952</threshold>
        <left_val>0.4507646858692169</left_val>
        <right_val>-0.4217903017997742</right_val></_></_>
<_>
```

Listing 5.4: Haar Cascade XML Feature

### 5.5.1 Cascade Implementation

Each Haar Cascade is implemented using the OpenCV method detectMultiScale which detects objects of different sizes in the input image. The detected objects are then returned as an array of rectangles which can be drawn around to object to indicate its detection. This method takes certain parameters that facilitate the interchanging of Haar Cascades. The EZ-B generic robotics IDE was used to implement Haar Cascade tracking owing to the ease of Haar Cascade interchangability. The EZ-B provides the function of loading any Haar Cascade into its tracking algorithm. The Haar Cascade need only be in the XML format so that custom objects may be tracked. The Haar Cascades used in this implementation can be found online at (OpenCV, 2013a). Figure 5.3 depicts the output of the eye pair, face and upper body Haar Cascades.

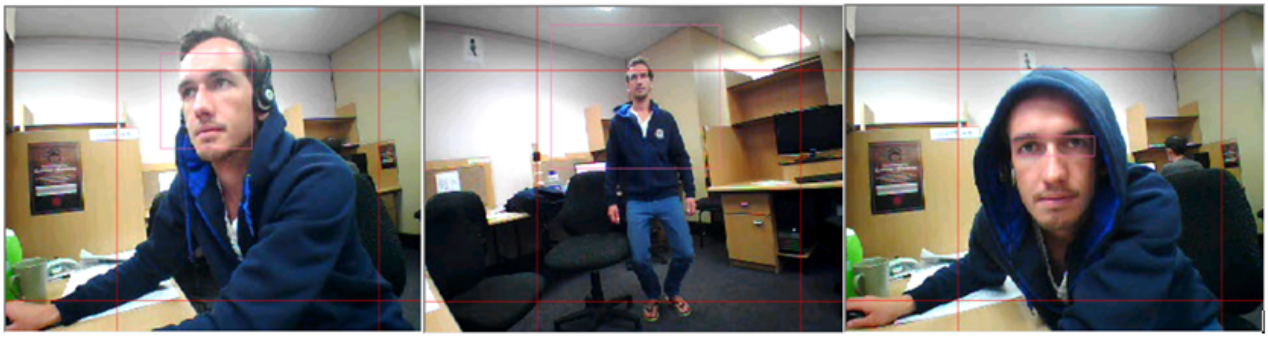

Figure 5.3: Haar Cascade Tracking: Face, Upper Body and Eye Pair

## 5.6 Setting up Glyph Recognition

Glyph recognition uses grey scaling, thresholding and quadrilateral transformation to to detect glyphs. These glyphs are then recognised by reconstructing the matrix of the glyph using dilation and erosion within given grid lines as mentioned in Section 4.4. Glyph detection and recognition are implemented using the EZ-B interface so that the grid style tracking as mentioned in Section 5.4 can be implemented. This interface also provides a scripting facility so that each of the glyphs can initiate the execution of custom code. Four glyphs are used in this implementation and can be seen in Figure 5.4.

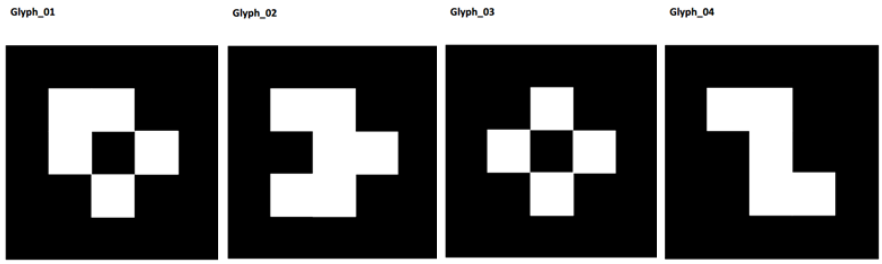


Figure 5.4: Implemented Glyphs

When a glyph is detected in one of the video stream frames it is extracted using the methods outlined in Section 4.4 and then displayed in the video feed in the top left hand corner of the video stream as feed back to the user. Each glyph needs to be loaded into the EZ-B before it can be recognised by the algorithm. Once loaded, the user can create scripts for each glyph and the grid tracking algorithm can be applied.

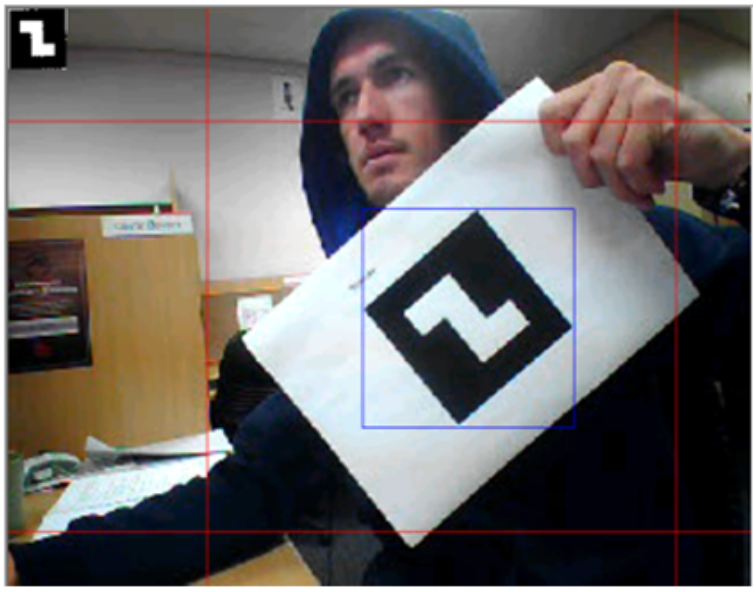

Figure 5.5: Glyph Detection and Recognition

## 5.7 Face recognition using Fisherfaces

The first step in implementing a face recognition program is to acquire a database of face images. This implementation makes use of the AT&T Facedatabase (Cambridge, 2002) with the addition of some new faces. The AT&T database contains face images of 40 different people. Each person has ten different images of their faces in the database. Each picture was taken at different times and is subject to different lighting conditions and facial expressions. The facial expressions can be of someone with their mouth open, closed or smiling, . Facial details in the photos also changes as some pictures are of the subject wearing glasses where others are not. All images in the AT&T Facedatabase have been taken against a homogeneous, dark background with the subject in a upright, front facing position. In addition to the AT&T Facedatabase images, three additional subjects were added to the photo collection.

### 5.7.1 Creating a Custom Image Database

The images added to the existing AT&T needed to be edited. This editing was done by cropping the face according to the position of the subjects eyes. This editing allows the Fisherfaces algorithm to focus on extracting features from the face that are robust to illumination, background interference and changes in the subject's hair. A python script was use to perform this editing. The cropping

function also served to reduce the size of the sample images to a standard size of 70x70 pixels that is used in the AT&T Facedatabase. The cropping function can be found in appendix XX and the changes to images can be seen in Figure 5.6.

Figure 5.6: Face Cropping Output

The face images needed to be stored in a specific file structure for the Fisherfaces algorithm to group samples of the same face as well as to provide a label to be returned when a specific face is recognised. This file structure required all images of the same face to be contained in a separate folder. These folders are then required to be contained within a separate folder. This one folder is then referenced as the single folder for the Fisherfaces algorithm to model faces. The file structure of the face images is illustrated in Figure 5.7.

```
philipp@mango:~/facerec/data/at$ tree
.
|-- README
|-- s1
|   |-- 1.pgm
|   |-- ...
|   |-- 10.pgm
|-- s2
|   |-- 1.pgm
|   |-- ...
|   |-- 10.pgm
...
|-- s40
|   |-- 1.pgm
|   |-- ...
|   |-- 10.pgm
```

Figure 5.7: Face Images File Structure

The Fisherfaces code implementation used here, created by Philipp Wagner (Wagner, 2012), learns a class-specific transformation matrix. This helps to reduce the impact that illumination has on the sample images used to recognise faces. The Discriminant Analysis finds the facial features in each sample image in order to tell two different faces apart. It should be noted that the Fisherface

algorithm's performance strongly relies on the input data. That is to say, in practice, the Fisherfaces algorithm will not perform well if the sample pictures used to train Fisherfaces are taken in a well illuminated environment and the faces that are trying to be recognised are input from a badly illuminated environment. This occurs as the features that are predominant in an image differ when in environments with vastly different lighting conditions.

# Chapter 6

# Testing and Analysis

This chapter details the various tests performed with the AR Drone to assess the capabilities of each algorithm with respect to detection, tracking and recognition. This chapter is split into four parts: detection testing, detection at angles, recognition testing and tracking testing.

## 6.1 Detection Testing

To assess the effectiveness of each algorithm with respect to its detection ability, a standard test was devised. Each algorithm needed to track its respective face, object or marker, hence forth known as the subject. The subject was placed a specific distance away from the camera and executed a standard set of movements. Each algorithm's detection ability was then assessed according to the number of frames the subject was detected in, the number of frames in which false detections (false positives) occured, the rate of false positives and the rate of true positives. The following sections will report on the performance of each algorithm and outline the specifics of each test.

### 6.1.1 Viola Jones Detection Results

The Viola Jones face detection algorithm uses a cascade of weak classifiers (Haar-like features) to identify a face according to predominant human facial features. The goal of this algorithm is to detect a human face in a live video stream. This test has been formulated to test the effectiveness of the Viola Jones face detection algorithm. The following tests were performed using the EZ-B robotics API. The subject the test is performed on starts off directly facing the camera in a seated position. This position is held for five seconds. The subject then leans to the left and holds this

position for five seconds. The subject then leans to the right and holds this position for five seconds. The subject then centers their face and stands up for five seconds. Lastly, the subject sits back down and holds this position for five seconds. The video stream detects at an average of six frames per second.

### Test 1

Test one placed the subject of detection at 1m away from the AR Drone's camera. The resolution of the video stream was set at 320x240. At this distance the subject's tracking box appeared in the video stream at a size of 47x47 pixels. The subject directly faces the camera. The test was performed three times using the above mentioned conditions. The results are detailed in Table 6.2.

| Epoch # | Seconds | Total frames | # True positives | # False positives | % False positives | % True positives |
|---|---|---|---|---|---|---|
| 1 | 25 | 150 | 138 | 6 | 4.00% | 92.00% |
| 2 | 25 | 150 | 132 | 3 | 2.00% | 88.00% |
| 3 | 25 | 150 | 128 | 5 | 3.33% | 85.33% |

Table 6.1: Viola Jones Detection Results: 1m

The algorithm accurately picks up faces in 88.4% of frames on average at this distance. There are a small number of frames in which false positives occurred. These false positives are expected to increase as the subject moves further from the camera.

### Test 2

Test two placed the subject of detection at 2m away from the AR Drone's camera. The resolution of the video stream was set at 320x240. At this distance the subject's tracking box appeared in the video stream at a size of 21x21 pixels. The subject directly faces the camera. The test was performed three times using the above mentioned conditions. The results are detailed in Table 6.2.

| Epoch # | Seconds | Total frames | # True positives | # False positives | % False positives | % True positives |
|---|---|---|---|---|---|---|
| 1 | 26 | 156 | 132 | 12 | 7.69% | 84.62% |
| 2 | 26 | 156 | 126 | 18 | 11.54% | 80.77% |
| 3 | 26 | 156 | 146 | 4 | 2.56% | 93.59% |

Table 6.2: Viola Jones Detection Results: 2m

The algorithm accurately picks up faces in 86.2% of frames on average at this distance. The algorithm makes more detections per frame than in test one. This suggests that the weak classifiers can match a face with higher frequency at 2m from the camera. The number of frames in which false positives occur increases at 2m. This is expected as there is more background in the video stream that can

cause interference in the video stream. These false positives are expected to increase as the subject moves further from the camera.

### Test 3

Test three placed the subject of detection at 3m away from the AR Drone's camera. The resolution of the video stream was set at 320x240. At this distance the subject's tracking box appeared in the video stream at a size of 15x15 pixels. The subject directly faces the camera. The test was performed three times using the above mentioned conditions. The results are detailed in Table 6.3.

| Epoch # | Seconds | Total frames | # True positives | # False positives | % False positives | % True positives |
|---|---|---|---|---|---|---|
| 1 | 25 | 150 | 96 | 36 | 24.00% | 64.00% |
| 2 | 25 | 150 | 84 | 30 | 20.00% | 56.00% |
| 3 | 25 | 150 | 90 | 42 | 28.00% | 60.00% |

Table 6.3: Viola Jones Detection Results: 3m

The algorithm accurately picks up faces in 60% of frames on average at this distance. The number of frames in which false positives occurred increases again at 3m. This is expected as there is more background in the video stream that can cause interference in the video stream. These false positives are expected to increase as the subject moves further from the camera.

### Test 4

Test four placed the subject of detection at 5m away from the AR Drone's camera. The resolution of the video stream was set at 320x240. The subject directly faces the camera. The test was performed three times using the above mentioned conditions. The results are detailed in Table 6.4.

| Epoch # | Seconds | Total frames | # True positives | # False positives | % False positives | % True positives |
|---|---|---|---|---|---|---|
| 1 | 25 | 150 | 6 | 72 | 48.00% | 4.00% |
| 2 | 25 | 150 | 10 | 64 | 42.67% | 6.67% |
| 3 | 25 | 150 | 7 | 70 | 46.67% | 4.67% |

Table 6.4: Viola Jones Detection Results: 5m

The algorithm accurately picks up faces in 5.1% of frames on average at this distance. The number of frames in which false positives occurred dramatically increases again at 5m. Over 89% of all detections were false positives. Evidently the Viola Jones face detection algorithm is ineffective in detecting faces at five metres and therefore will not be suitable for use in face tracking.

### Viola Jones Detection Test Summary

The Viola Jones face detection algorithm is effective at detecting faces at this frame rate and pixel density up to a distance of three metres. Beyond three metres the algorithm detects more false positives than true positives. The relationship of correct detection to distance is illustrated in Figure 6.1.

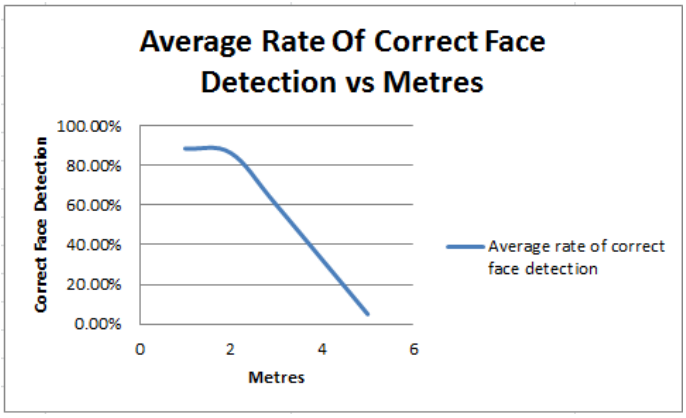


Figure 6.1: Viola Jones Detection Results Graph

### 6.1.2 CamShift Detection Results

The CamShift algorithm performs detection by using the user specified values of Hue, Saturation and Value to detect an object. The algorithm that detects the object does so by finding the largest contour in a binary image. The goal of this algorithm is to detect an object in a live video stream according to its colour. This test has been designed to test the effectiveness of the CamShift algorithm at different distances. The following tests were performed using OpenCV and the CVDrone library. The subject the test is performed on starts off in the centre of the video stream. This position is held for five seconds. The subject is then moved to the left and is held in this position for five seconds. The subject is then moved to the right and holds this position for five seconds. The subject is then raised for five seconds. Lastly, the subject is lowered and held in this position for five seconds. The video stream detects at an average of six frames per second. The HSV values of the CamShift algorithm are set to detect a distinctively red ball.

#### Test 1

Test one placed the subject of detection at 1m away from the AR Drone's camera. The resolution of the video stream was set at 640x480. At this distance the subject's tracking box appeared in

the video stream at a size of 30x30 pixels. As the subject of detection is round, the angle it faces the camera is negligible. The test was performed three times using the above mentioned conditions. The results are detailed in Table 6.6.

| Epoch # | Seconds | Total frames | # True positives | # False positives | % False positives | % True positives |
|---|---|---|---|---|---|---|
| 1 | 25 | 150 | 150 | 0 | 0.00% | 100.00% |
| 2 | 25 | 150 | 150 | 0 | 0.00% | 100.00% |
| 3 | 25 | 150 | 150 | 0 | 0.00% | 100.00% |

Table 6.5: CamShift Detection Results: 1m

The algorithm accurately picks up the object in 100% of frames on average at this distance.The are no false positives at this distance. This can be attributed to the distinct colour of the object. False positives are only expected to occur at further distances where other objects with a similar colouration enter the frame. These false positives will only occur where the contours of the similarly coloured object are larger than that of the subject.

### Test 2

Test two placed the subject of detection at 3m away from the AR Drone's camera. The resolution of the video stream was set at 640x480. At this distance the subject's tracking box appeared in the video stream at a size of 12x12 pixels. As the subject of detection is round, the angle it faces the camera is negligible. The test was performed three times using the above mentioned conditions. The results are detailed in Table 6.6.

| Epoch # | Seconds | Total frames | # True positives | # False positives | % False positives | % True positives |
|---|---|---|---|---|---|---|
| 1 | 25 | 150 | 132 | 18 | 12.00% | 88.00% |
| 2 | 25 | 150 | 138 | 12 | 8.00% | 92.00% |
| 3 | 25 | 150 | 126 | 24 | 16.00% | 84.00% |

Table 6.6: CamShift Detection Results: 3m

The algorithm accurately picks up the object in 88% of frames on average at this distance. The are very few false positives at this distance. This can be attributed to the distinct colour of the object. These false positives occurred when the subject was raised into the air. This can be attributed to the glare from the fluorescent lights in the video feed. The lights change the saturation of the ball in the video feed and this causes the algorithm to lose detection of the ball. This loss is illustrated well in the back propagation video stream. A larger number of false positives are expected to occur at further distances where other objects with a similar colouration enter the frame. These false positives will only occur where the contours of the similarly coloured object are larger than that of the subject.

### Test 3

Test three placed the subject of detection at 5m away from the AR Drone's camera. The resolution of the video stream was set at 640x480. At this distance the subject's tracking box appeared in the video stream at a size of 7x7 pixels. As the subject of detection is round, the angle it faces the camera is negligible. The test was performed three times using the above mentioned conditions. The results are detailed in Table 6.7.

| Epoch # | Seconds | Total frames | # True positives | # False positives | % False positives | % True positives |
|---|---|---|---|---|---|---|
| 1 | 25 | 150 | 126 | 24 | 16.00% | 84.00% |
| 2 | 25 | 150 | 131 | 19 | 12.67% | 87.33% |
| 3 | 25 | 150 | 129 | 21 | 14.00% | 86.00% |

Table 6.7: CamShift Detection Results: 5m

The algorithm accurately picks up the object in 85.7% of frames on average at this distance.The are very few false positives at this distance. This can be attributed to the distinct colour of the object. These false positives occurred when the subject was raised into the air. This can be attributed to the glare from the fluorescent lights in the video feed. The lights change the saturation of the ball in the video feed and this causes the algorithm to lose the image of the ball. This loss is illustrated well in the back propagation video stream. False positives also occurred due to a similarly coloured object entering the video stream (a fire bell). A larger number of false positives are expected to occur at further distances owing to the increased likelihood of objects with a similar colouration entering the video stream. These false positives will only occur where the contours of the similarly coloured object are larger than that of the subject.

### Test 4

Test four placed the subject of detection at 8m away from the AR Drone's camera. The resolution of the video stream was set at 640x480. At this distance the subject's tracking box appeared in the video stream at a size of 4x4 pixels. As the subject of detection is round, the angle it faces the camera is negligible. The test was performed three times using the above mentioned conditions. The results are detailed in Table 6.8.

| Epoch # | Seconds | Total frames | # True positives | # False positives | % False positives | % True positives |
|---|---|---|---|---|---|---|
| 1 | 25 | 150 | 96 | 30 | 20.00% | 64.00% |
| 2 | 25 | 150 | 102 | 42 | 28.00% | 68.00% |
| 3 | 25 | 150 | 108 | 38 | 25.33% | 72.00% |

Table 6.8: CamShift Detection Results: 5m

The algorithm accurately picks up the object in 68% of frames on average at this distance. More false positives occur at this distance. This can be attributed to more similarly objects entering the video stream. These false positives occurred again when the subject was raised into the air. This can be attributed to the glare from the fluorescent lights in the video feed. The lights change the saturation of the ball in the video feed and this causes the algorithm to lose the image of the ball. This loss is illustrated well in the back propagation video stream. False positives due to similarly coloured object entering the video stream (a fire bell, a pair of red shoes). With the subject at a greater distance from the camera, the contours of the similarly coloured objects can become larger than that of the subject. This accounts for the majority of false positives that occurred.

### CamShift Detection Test Summary

The CamShift algorithm performs effectively when tracking a distinctly coloured object at this frame rate and pixel density up to a distance of five metres. The CamShift algorithm produces considerably less false positives than the Viola Jones face detection algorithm. This remains true even when the subject of detection is further away from the camera. The use of OpenCV and the CVDrone library maintained a more stable video feed than the EZ-B as there were fewer instances of the video feed crashing. There were also fewer instances of video feed transmission delay between the drone and the client program. According to these results, it is assumed that CamShift will be a robust algorithm to implement tracking. The relationship of correct detection to distance using the CamShift algorithm is illustrated in Figure 6.2.

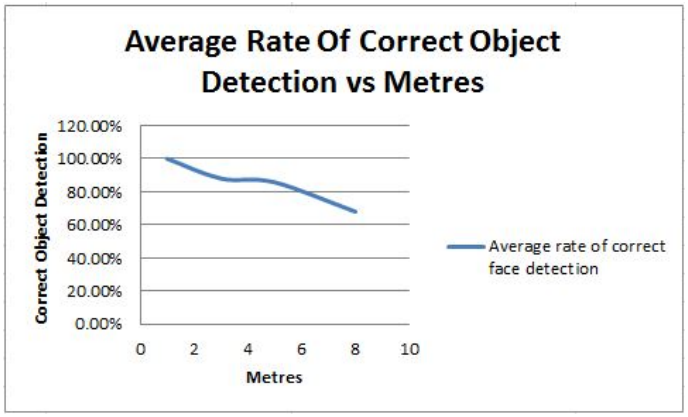


Figure 6.2: CamShift Detection Results Graph

### 6.1.3 Various Haar Cascade Detection Results

The following tests assessed the detection capabilities of various Haar Cascades. Each cascade contains a number of weak classifiers (Haar-like features) to identify a human according to predominant human features. The goal of this algorithm is to detect part of human in a live video stream. The following tests were performed using the OpenCV Haar Cascades and the EZ-B robotics SDK. Each test was performed differently according to which part of the human body being tracked. The video stream in these tests detects at an average of six frames per second.

#### Eye Detection Haar Cascade Detection Results

The eye detection Haar Cascade uses a cascade of weak classifiers (Haar-like features) to detect the position of a pair of eyes according to predominant human facial features. This test has been formulated to test the effectiveness of the eyes detection Haar Cascade algorithm. The subject the test is performed on starts off directly facing the camera in a seated position approximately 1m away from the camera. This position is held for five seconds. The subject then leans to the left and holds this position for five seconds. the subject then leans to the right and holds this position for five seconds. This movement is performed twice in each epoch of the test. The test was performed three times using the eye detection Haar Cascade. The results are detailed in Table 6.9.

| Epoch # | Seconds | Total frames | # True positives | # False positives | % False positives | % True positives |
|---|---|---|---|---|---|---|
| 1 | 22 | 132 | 20 | 0 | 0.00% | 15.15% |
| 2 | 21 | 126 | 21 | 0 | 0.00% | 16.67% |
| 3 | 21 | 126 | 19 | 0 | 0.00% | 15.08% |

Table 6.9: Eyes Detection Results: 1m

The eyes detection Haar Cascade tests produced poor results. The algorithm was not able to detect a pair of eyes other than in ideal circumstances. The subject's eyes needed to be very close to the camera and in the centre of the video feed for the algorithm to pick up the eyes. The algorithm was unable to detect the eyes when in motion or when the eyes were to the left or right of the screen. This being said, no false detections occurred. The algorithm was only able to accurately pick up a pair of eyes in 15.6% of frames on average at this distance.

#### Face Detection Haar Cascade

The face detection Haar Cascade uses a cascade of weak classifiers (Haar-like features) to detect the position of a face according to predominant human facial features. This test has been formulated

to test the effectiveness of the face detection Haar Cascade algorithm. The subject the test is performed on starts off directly facing the camera in a seated position approximately 2m away from the camera. This distance was chosen as efficient results were produced at a similar distance in the Viola Jones testing. The subject the test is performed on starts off directly facing the camera in a seated position. This position is held for five seconds. The subject then leans to the left and holds this position for five seconds. The subject then leans to the right and holds this position for five seconds. The subject then centres their face and stands up for five seconds. Lastly, the subject sits back down and holds this position for five seconds. The test was performed three times using the face detection Haar Cascade. The results are detailed in Table 6.10.

| Epoch # | Seconds | Total frames | # True positives | # False positives | % False positives | % True positives |
|---|---|---|---|---|---|---|
| 1 | 31 | 180 | 145 | 32 | 17.78% | 80.56% |
| 2 | 30 | 186 | 148 | 30 | 16.13% | 79.57% |
| 3 | 32 | 192 | 150 | 35 | 18.23% | 78.13% |

Table 6.10: Face Detection Results: 1m

The algorithm accurately picks up faces in 79.42% of frames on average at this distance. This is slightly less effective than the Viola Jones face detection algorithm at 2m. The number of frames in which false positives occur is also greater than the number false positive frames in the Viola Jones algorithm.

### Upper Body Detection Haar Cascade

The upper body detection Haar Cascade uses a cascade of weak classifiers (Haar-like features) to detect the position of a human upper body according to predominant human features. This test has been formulated to test the effectiveness of the upper body detection Haar Cascade algorithm. The subject the test is performed on starts off directly facing the camera in a standing position approximately 2.5m away from the camera. This position is held for five seconds. The subject then moves to the left and holds this position for five seconds. The subject then moves to the right and holds this position for five seconds. The subject then centres their body for five seconds. This movement is performed twice. The test was performed three times using the upper body detection Haar Cascade. The results are detailed in Table 6.11.

| Epoch # | Seconds | Total frames | # True positives | # False positives | % False positives | % True positives |
|---|---|---|---|---|---|---|
| 1 | 29 | 154 | 138 | 26 | 16.88% | 89.61% |
| 2 | 30 | 160 | 130 | 25 | 15.63% | 81.25% |
| 3 | 30 | 160 | 131 | 29 | 18.13% | 81.88% |

Table 6.11: Upper Body Detection Results: 2.5m

The algorithm accurately picks the upper body in 84.24% of frames on average at this distance. This cascade performed well at this distance. However, the algorithm detected multiple upper bodys in the video stream when there was only one present. These false positives lead to a high rate of upper body detection which can be a misleading figure. This algorithm performs well at 2.5m but is expected to deteriourate rapidly as the drone closes the space between itself and the subject. Figure 6.3 illustrates the detection results of each Haar Cascade.

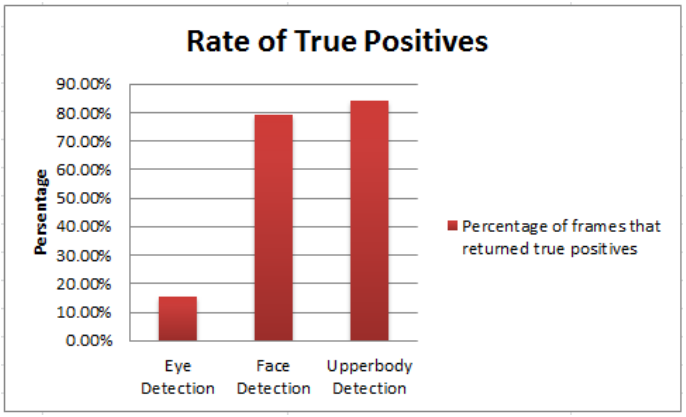


Figure 6.3: Haar Cascade Detection Results Graph

## 6.2 Detection at Angles

This section details the tests performed too assess an algorithms ability to detect an object, human feature or fiducial marker at an angle. A standard test was formulated to assess the effectiveness of each algorithm. The test results from the detection section were used to determine the distance the subject would be from the camera. The distance at which each algorithm performed best was used to test the algorithm's ability to detect the subject at various angles.

### Viola Jones Detection Angle Testing

This test has been formulated to test the effectiveness of the Viola Jones face detection algorithm. In particularly the angle at which a face can be detected. The video streams images at an average of 6 frames per second using a pixel density of 320x240. The face is placed at 1m away as previous testing at this distance, with this algorithm, produced accurate detection results. This test is performedby initially detecting a face from a flat angle. This face/object is then rotated in increments of 15 degrees to a maximum of 90 degrees. The face/object is held at each respective increment for 5

seconds to measure the detection effectiveness. Results of this test are illustrated in Table 6.12.

| Test Angle (degrees) | Seconds | Total frames | # True positives | # False positives | % False positives | % True positives |
|---|---|---|---|---|---|---|
| 15 | 5 | 30 | 30 | 0 | 0.00% | 100.00% |
| 30 | 5 | 30 | 30 | 0 | 0.00% | 100.00% |
| 45 | 5 | 30 | 18 | 12 | 40.00% | 60.00% |
| 60 | 5 | 30 | 6 | 18 | 60.00% | 20.00% |
| 75 | 5 | 30 | 0 | 3 | 10.00% | 0.00% |
| 90 | 5 | 30 | 0 | 12 | 40.00% | 0.00% |

Table 6.12: Viola Jones Angle Testing Results: 1m

Viola Jones was able to maintain detection of the subject effectively up to 45 degrees. Beyond this point the subject cannot be detected consistently. This indicates that this algorithm will be able track a subject at any front facing offset of up to 45 degrees when tracking.

### CamShift Detection Angle Testing

This test has been formulated to test the effectiveness of the CamShift detection algorithm. In particularly the angle at which an object can be detected. The video streams images at an average of 6 frames per second using a pixel density of 640x480. The object is placed at 1m away as previous testing at this distance, with this algorithm, produced accurate detection results. This test is performed by initially detecting an object from a flat angle. This object is then rotated in increments of 15 degrees to a maximum of 90 degrees. The object is held at each respective increment for 5 seconds to measure the detection effectiveness. Previous testing with the CamShift algorithm made use of a round red ball which was not suitable for angle testing. This test made use of a piece of red, rectangular foam. Results of this test are illustrated in Table 6.13.

| Test Angle (degrees) | Seconds | Total frames | # True positives | # False positives | % False positives | % True positives |
|---|---|---|---|---|---|---|
| 15 | 5 | 30 | 30 | 0 | 0.00% | 100.00% |
| 30 | 5 | 30 | 30 | 0 | 0.00% | 100.00% |
| 45 | 5 | 30 | 30 | 0 | 0.00% | 100.00% |
| 60 | 5 | 30 | 30 | 0 | 0.00% | 100.00% |
| 75 | 5 | 30 | 27 | 3 | 10.00% | 90.00% |
| 90 | 5 | 30 | 0 | 0 | 0.00% | 0.00% |

Table 6.13: CamShift Angle Testing Results: 1m

CamShift is able to maintain detection of the subject effectively up to 75 degrees. Beyond this point the subject cannot be detected. This indicates that this algorithm will be able track a subject at any front facing offset of up to 75 degrees when tracking. This algorithm is very effective as it only needs the presence of the colour being tracked unlike Haar Cascades which require various arrangements of light and dark pixels.

## Fiducial Marker Detection Angle Testing

This test has been formulated to test the effectiveness of the Fiducial Marker detection algorithm. In particularly the angle at which a marker can be detected. The video streams images at an average of 6 frames per second using a pixel density of 320x240. The face is placed at 1m away as previous testing at this distance, with this algorithm, produced accurate detection results. This test is performed by initially detecting a marker from a flat angle. This face/object is then rotated in increments of 15 degrees to a maximum of 90 degrees. The marker is held at each respective increment for 5 seconds to measure the detection effectiveness. Results of this test are illustrated in Table 6.14.

| Test Angle (degrees) | Seconds | Total frames | # True positives | # False positives | % False positives | % True positives |
|---|---|---|---|---|---|---|
| 15 | 5 | 30 | 30 | 0 | 0.00% | 100.00% |
| 30 | 5 | 30 | 27 | 0 | 0.00% | 90.00% |
| 45 | 5 | 30 | 0 | 0 | 0.00% | 0.00% |
| 60 | 5 | 30 | 0 | 0 | 0.00% | 0.00% |
| 75 | 5 | 30 | 0 | 0 | 0.00% | 0.00% |
| 90 | 5 | 30 | 0 | 0 | 0.00% | 0.00% |

Table 6.14: Fiducial Marker Angle Testing Results: 1m

Viola Jones is able to maintain detection of the subject effectively up to 30 degrees. Beyond this point the subject cannot be detected consistently. This indicates that this algorithm will be able track a subject at any front facing offset of up to 30 degrees when tracking. The algorithms ability to detect quadrilaterals deteriorates rapidly when the image is rotated. The algorithm also finds it difficult to reconstruct the matrix of a marker beyond 30 degrees as the image becomes too warped during quadrilateral transformation to determine matrix values.

## Eyes Detection Angle Testing

This test has been formulated to test the effectiveness of the eyes detection Haar Cascade algorithm. In particularly the angle at which a pair of eyes can be detected. The video streams images at an average of 6 frames per second using a pixel density of 320x240. The face is placed at 1m away as previous testing at this distance, with this algorithm, produced the most accurate detection results. This test is performed by initially detecting a pair of eyes from a flat angle. This face is then rotated in increments of 15 degrees to a maximum of 90 degrees. The face is held at each respective increment for 5 seconds to measure the detection effectiveness. Results of this test are illustrated in Table 6.15.

| Test Angle (degrees) | Seconds | Total frames | # True positives | # False positives | % False positives | % True positives |
|---|---|---|---|---|---|---|
| 15 | 5 | 30 | 6 | 0 | 0.00% | 20.00% |
| 30 | 5 | 30 | 0 | 0 | 0.00% | 0.00% |
| 45 | 5 | 30 | 0 | 0 | 0.00% | 0.00% |
| 60 | 5 | 30 | 0 | 0 | 0.00% | 0.00% |
| 75 | 5 | 30 | 0 | 0 | 0.00% | 0.00% |
| 90 | 5 | 30 | 0 | 0 | 0.00% | 0.00% |

Table 6.15: Eyes Angle Testing Results: 1m

Eyes detection Haar Cascade is not able to maintain detection of the subject effectively other than at a flat angle. This indicates that this algorithm not suitable for use in subject tracking. The rate of correct object detection is far too low to perform well in any quadrotor tracking environment. This algorithm will not be used further in testing.

## Face Detection Angle Testing

This test has been formulated to test the effectiveness of the face detection Haar Cascade algorithm. In particularly the angle at which a face can be detected. The video streams images at an average of 6 frames per second using a pixel density of 320x240. The face is placed at 1m away as previous testing at this distance, with this algorithm, produced accurate detection results. This test is performed by initially detecting a face from a flat angle. This face is then rotated in increments of 15 degrees to a maximum of 90 degrees. The face is held at each respective increment for 5 seconds to measure the detection effectiveness. Results of this test are illustrated in Table 6.16.

| Test Angle (degrees) | Seconds | Total frames | # True positives | # False positives | % False positives | % True positives |
|---|---|---|---|---|---|---|
| 15 | 5 | 30 | 30 | 0 | 0.00% | 100.00% |
| 30 | 5 | 30 | 30 | 0 | 0.00% | 100.00% |
| 45 | 5 | 30 | 27 | 3 | 10.00% | 90.00% |
| 60 | 5 | 30 | 24 | 0 | 0.00% | 80.00% |
| 75 | 5 | 30 | 0 | 12 | 40.00% | 0.00% |
| 90 | 5 | 30 | 0 | 12 | 40.00% | 0.00% |

Table 6.16: Face Angle Testing Results: 1m

The face detection Haar Cascade is able to maintain detection of the subject effectively up to 60 degrees. Beyond this point the subject cannot be detected consistently. This indicates that this algorithm will be able track a subject at any front facing offset of up to 60 degrees when tracking.

### Upper Body Detection Angle Testing

This test has been formulated to test the effectiveness of the upper body detection Haar Cascade algorithm. In particularly the angle at which an upper body can be detected. The video streams images at an average of 6 frames per second using a pixel density of 320x240. The subject is placed

at 2.5m away as previous testing at this distance, with this algorithm, produced accurate detection results. This test is performed by initially detecting an upper body from a flat angle. The upper body is then rotated in increments of 15 degrees to a maximum of 90 degrees. The upper body is held at each respective increment for 5 seconds to measure the detection effectiveness. Results of this test are illustrated in Table 6.17.

| Test Angle (degrees) | Seconds | Total frames | # True positives | # False positives | % False positives | % True positives |
|---|---|---|---|---|---|---|
| 15 | 5 | 30 | 27 | 3 | 10.00% | 90.00% |
| 30 | 5 | 30 | 18 | 12 | 40.00% | 60.00% |
| 45 | 5 | 30 | 15 | 15 | 50.00% | 50.00% |
| 60 | 5 | 30 | 18 | 12 | 40.00% | 60.00% |
| 75 | 5 | 30 | 6 | 24 | 80.00% | 20.00% |
| 90 | 5 | 30 | 6 | 24 | 80.00% | 20.00% |

Table 6.17: Upper Body Angle Testing Results: 1m

The upper body detection Haar Cascade is able to maintain detection of the subject effectively up to 60 degrees. Beyond this point the subject cannot be detected consistently. This indicates that this algorithm will be able track a subject at any front facing offset of up to 60 degrees when tracking.

## 6.3 Recognition Results

To assess the effectiveness of each of the recognition algorithms, a standard test was devised. Each algorithm needed to recognise its respective face, object or marker, hence forth known as the subject. The subject was placed a specific distance away from the camera and executed a standard set of movements. Each algorithm's recognition ability was then assessed according to the number of frames the subject was detected in (true positives), the number of frames in which false detections (false positives) were made, the overall percentage of false positives and the overall percentage of true positives. The following sections will report on the performance of each algorithm and outline the specifics of each test.

### 6.3.1 Fiducial Marker Recognition Results

The fiducial marker recognition algorithm uses the quadrilateral transformation algorithm and fiducial marker matrix reconstruction algorithm to recognise a marker. The goal of this algorithm is to detect and identify a fiducial marker in a live video stream. The following tests were performed using the EZ-B robotics API. The subject the test is performed on starts off directly facing the camera. This position is held for five seconds. The subject then moves to the left and holds this position for five seconds. The subject then moves to the right and holds this position for five seconds. The

subject is then centred and raised for five seconds. Lastly the subject is lowered and is held in this position for five seconds. The video stream detects at an average of six frames per second.

### Test 1

Test one placed the subject of recognition at 1m away from the AR Drone's camera. The resolution of the video stream was set at 320x240. At this distance the subject's tracking box appeared in the video stream at a size of 47x47 pixels. The subject directly faces the camera. This test was performed three times using the above mentioned conditions. The results are detailed in Table 6.19.

| Epoch # | Duration (Seconds) | Total # of frames | # True positive frames | # False positive frames | % False positive frames | % True positive frames |
|---|---|---|---|---|---|---|
| 1 | 28 | 168 | 138 | 0 | 0.00% | 82.14% |
| 2 | 28 | 168 | 131 | 0 | 0.00% | 77.98% |
| 3 | 28 | 168 | 133 | 0 | 0.00% | 79.17% |

Table 6.18: Fiducial Marker Recognition Results: 1m

The algorithm accurately picks up the marker in 79.76% of frames on average at this distance. There are no false positives that occur as a fiducial marker is a very distinct image.

### Test 2

Test two placed the subject of recognition at 1.5m away from the AR Drone's camera. The resolution of the video stream was set at 320x240. At this distance the subject's tracking box appeared in the video stream at a size of 47x47 pixels. The subject directly faces the camera. This test was performed three times using the above mentioned conditions. The results are detailed in Table 6.19.

| Epoch # | Duration (Seconds) | Total # of frames | # True positive frames | # False positive frames | % False positive frames | % True positive frames |
|---|---|---|---|---|---|---|
| 1 | 24 | 144 | 90 | 0 | 0.00% | 62.50% |
| 2 | 25 | 150 | 66 | 0 | 0.00% | 44.00% |
| 3 | 25 | 150 | 66 | 0 | 0.00% | 44.00% |

Table 6.19: Fiducial Marker Recognition Results: 1.5m

The algorithm accurately picks up the marker in 50.16% of frames on average at this distance.There are no false positives that occur as a fiducial marker is a very distinct image.

### Test 3

Test three placed the subject of recognition at 2m away from the AR Drone's camera. The resolution of the video stream was set at 320x240. At this distance the subject's tracking box appeared in the video stream at a size of 47x47 pixels. The subject directly faces the camera. This test was performed three times using the above mentioned conditions. The results are detailed in Table 6.20.

| Epoch # | Duration (Seconds) | Total # of frames | # True positive frames | # False positive frames | % False positive frames | % True positive frames |
|---|---|---|---|---|---|---|
| 1 | 23 | 138 | 12 | 0 | 0.00% | 8.70% |
| 2 | 20 | 120 | 18 | 0 | 0.00% | 15.00% |
| 3 | 21 | 126 | 12 | 0 | 0.00% | 9.52% |

Table 6.20: Fiducial Marker Recognition Results: 2m

The algorithm accurately picks up the marker in 11.07% of frames on average at this distance. There are no false positives that occur as a fiducial marker is a very distinct image.

### Fiducial Marker Recognition Summary

Fiducial markers effective tracking mechanism at close range and produce no false positives. However, beyond 2m these markers are unable to be detected. The lack of false positives makes fiducial markers a reliable mechanism to issue flight commands to the AR Drone as it is highly unlikely that one marker will be recognised as another. It is expected that this depends on the number of fiducial markers that a detected marker is being compared against.

## 6.3.2 Fisherfaces Recognition Results

The Fisherfaces recognition algorithm uses dimension reducing methods to represent sample images of faces to train the algorithm to recognise faces. The goal of this algorithm is to recognise the face of a specific human in a live video stream. The following tests were performed using an OpenCV implementation of the Fisherfaces algorithm. This test has been formulated to test the effectiveness of the Fisherfaces face recognition algorithm. Three different subjects were used to perform these tests as one may produce bias results by using only one subject. The subject the test is performed on starts off directly facing the camera in a seated position. This position is held for five seconds. The subject then leans to the left and holds this position for five seconds. The subject then leans to the right and holds this position for five seconds. The subject then centers their face and rotates their head to the left for five seconds and then to the right for five seconds. The video stream detects at an average of 15 frames per second. In each of the test the subject sits at approximately 1m from the camera.

### Test 1

Test one performed recognition using a Fisherfaces algorithm trained to recognise two different faces. The resolution of the video stream was set at 640x480. This test was performed three times using one of the faces that was trained in the algorithm. The results are detailed in Table 6.22.

| Epoch # | Seconds | Total frames | # Face detected frames | # True recog. Frames | % True face det. | % True face recog. | % False face recog. |
|---|---|---|---|---|---|---|---|
| 1 | 25 | 375 | 345 | 320 | 92.00% | 85.33% | 6.67% |
| 2 | 27 | 405 | 370 | 360 | 91.36% | 88.89% | 2.47% |
| 3 | 29 | 435 | 405 | 390 | 93.10% | 89.66% | 3.45% |

Table 6.21: Fisherfaces Recognition Results: 2 Trained Faces

The algorithm recognises the face in 87.96% of frames on average. There are very few false positives that occur.

### Test 2

Test two performed recognition using a Fisherfaces algorithm trained to recognise three different faces. The resolution of the video stream was set at 640x480. This test was performed three times using all three of the faces that were trained in the algorithm. The results are detailed in Table 6.22.

| Epoch # | Seconds | Total frames | # Face detected frames | # True recog. Frames | % True face det. | % True face recog. | % False face recog. |
|---|---|---|---|---|---|---|---|
| 1 | 37 | 555 | 405 | 396 | 72.97% | 71.35% | 1.62% |
| 2 | 33 | 495 | 399 | 365 | 80.61% | 73.74% | 6.87% |
| 3 | 28 | 420 | 360 | 105 | 85.71% | 25.00% | 60.71% |

Table 6.22: Fisherfaces Recognition Results: 2 Trained Faces

The algorithm recognises the face in 56.70% of frames on average. There are a large number of false positive frames for one of the faces. This is caused by similar facial features of different faces or the algorithms inability to discriminate the class of this face in particular.

### Test 3

Test three performed recognition using a Fisherfaces algorithm trained to recognise five different faces. The resolution of the video stream was set at 640x480. This test was performed three times using three of the faces that were trained in the algorithm. The results are detailed in Table 6.23.

| Epoch # | Seconds | Total frames | # Face detected frames | # True recog. Frames | % True face det. | % True face recog. | % False face recog. |
|---|---|---|---|---|---|---|---|
| 1 | 36 | 540 | 275 | 255 | 50.93% | 47.22% | 3.70% |
| 2 | 30 | 450 | 390 | 5 | 86.67% | 1.11% | 85.56% |
| 3 | 27 | 405 | 405 | 0 | 100.00% | 0.00% | 100.00% |

Table 6.23: Fisherfaces Recognition Results: 5 Trained Faces

The algorithm recognises the face in 16.11% of frames on average. There are a large number of false positive frames for one of the faces. This is caused by similar facial features of different faces or the algorithms inability to discriminate the class of this face in particular. The face that cannot be recognised is the same face that could not be recognised in previous tests.

### Test 4

Test four performed recognition using a Fisherfaces algorithm trained to recognise 10 different faces. The resolution of the video stream was set at 640x480. This test was performed three times using three of the faces that were trained in the algorithm. The results are detailed in Table 6.24.

| Epoch # | Seconds | Total frames | # Face detected frames | # True recog. Frames | % True face det. | % True face recog. | % False face recog. |
|---|---|---|---|---|---|---|---|
| 1 | 20 | 300 | 300 | 0 | 100.00% | 0.00% | 100.00% |
| 2 | 25 | 375 | 322 | 230 | 85.87% | 61.33% | 24.53% |
| 3 | 25 | 375 | 323 | 15 | 86.13% | 4.00% | 82.13% |

Table 6.24: Fisherfaces Recognition Results: 10 Trained Faces

The algorithm recognises the face in 21.78% of frames on average. There are a large number of false positive frames for two of the faces.

### Test 5

Test five performed recognition using a Fisherfaces algorithm trained to recognise 20 different faces. The resolution of the video stream was set at 640x480. This test was performed three times using three of the faces that were trained in the algorithm. The results are detailed in Table 6.25.

| Epoch # | Seconds | Total frames | # Face detected frames | # True recog. Frames | % True face det. | % True face recog. | % False face recog. |
|---|---|---|---|---|---|---|---|
| 1 | 32 | 480 | 356 | 33 | 74.17% | 6.88% | 67.29% |
| 2 | 25 | 375 | 285 | 69 | 76.00% | 18.40% | 57.60% |
| 3 | 26 | 390 | 369 | 0 | 94.62% | 0.00% | 94.62% |

Table 6.25: Fisherfaces Recognition Results: 20 Trained Faces

The algorithm recognises the face in 8.43% of frames on average. There are a large number of false positive frames for all three of the faces.

### Test 6

Test six performed recognition using a Fisherfaces algorithm trained to recognise 43 different faces. The resolution of the video stream was set at 640x480. This test was performed three times using three of the faces that were trained in the algorithm. The results are detailed in Table 6.26.

| Epoch # | Seconds | Total frames | # Face detected frames | # True recog. Frames | % True face det. | % True face recog. | % False face recog. |
|---|---|---|---|---|---|---|---|
| 1 | 32 | 480 | 441 | 12 | 91.88% | 2.50% | 89.38% |
| 2 | 27 | 405 | 263 | 54 | 64.94% | 13.33% | 51.60% |
| 3 | 32 | 480 | 420 | 8 | 87.50% | 1.67% | 85.83% |

Table 6.26: Fisherfaces Recognition Results: 43 Trained Faces

The algorithm recognises the face in 8.43% of frames on average. There are a large number of false positive frames for all three of the faces.

### Fisherfaces Recognition Test Summary

This algorithm can recognise a face accurately when there are a few number of faces trained to the algorithm. The number of false recognitions that occur increase rapidly as the number of faces trained increases. The algorithm manages to detect a face with the same accuracy as the face detection Haar Cascade. The test results suggest that one face may produce very different results from another under the same training and testing conditions. This can be caused by a large similarity in facial features in different faces or by the algorithms inability to distinguish a face class from a set of others. The Fisherfaces algorithm is not used during tracking testing owing to the high number of false positives produced. The algorithm could be improved on by adding more sample images to the training data or by determining the optimal lighting conditions in which sample images should be taken to better train the Fisherfaces algorithm.

## 6.4 Tracking testing

To test the capability of each tracking algorithm during flight, a standard flight pattern was devised as a basis for algorithm comparrison. The most successful four algorithms in detection, angle and recognition testing were used to test tracking. These algorithms are were the Viola Jones, CamShift, Fiducial marker recognition and the upper body detection Haar Cascade. Each algorithm either tracks a face, object or marker which is referred to as the subject. The subject of each test is moved so that the flight pattern manoeuvres of the drone are as follows:

1. Take off.
2. Detect the subject.
3. Fly approximately 1-3 metres to the subject. Distance depends on algorithm capabilities.
4. Stop before colliding with the subject.
5. Track the subject as it circles the drone, completing a 180 degree rotation.
6. Follow the subject as it moves 3 metres away from the drone.
7. Adjust altitude as the subject ascends, then descends.

8. Land.

The subject of these tests moves at approximately 0.5m/s.

### 6.4.1 Viola Jones Tracking Results

The following tests were performed using the EZ-B robotics API. The video stream detects at an average of six frames per second. Tracking results are displayed in Table 6.27.

| Epoch # | Seconds | Total frames | # True positives | # False positives | % Overall detection | % True Positives | % False postives |
|---|---|---|---|---|---|---|---|
| 1 | 14 | 84 | 39 | 30 | 82.14% | 46.43% | 35.71% |
| 2 | 21 | 126 | 72 | 15 | 69.05% | 57.14% | 11.90% |
| 3 | 7 | 42 | 25 | 15 | 95.24% | 59.52% | 35.71% |
| 4 | 25 | 150 | 70 | 13 | 55.33% | 46.67% | 8.67% |
| 5 | 6 | 36 | 12 | 3 | 41.67% | 33.33% | 8.33% |
| 6 | 24 | 144 | 78 | 15 | 64.58% | 54.17% | 10.42% |
| 7 | 9 | 54 | 39 | 6 | 83.33% | 72.22% | 11.11% |
| 8 | 9 | 54 | 36 | 9 | 83.33% | 66.67% | 16.67% |

Table 6.27: Viola Jones Tracking Results

### Notes on each test Epoch

Epoch 1: Owing to the high number of false positives that the algorithm was detecting, the drone was executing commands based on non-face images, causing it to go off course.

Epoch 2: Tracked a face with effectiveness but again false positives led to the drone making incorrect flight decisions.

Epoch 3: Subject lost owing to a large flight correction in the direction of an object that returned a false positive.

Epoch 4: Successful flight. A second face in the video stream attracted the drone away from the primary subject.

Epoch 5: Successful flight. The drone took off and turned away from the subject but recovered rapidly. The EZ B lost the socket connection with the drone and so the video feed crashed. This halted the drone's execution of commands.

Epoch 6: A successful flight but still with too many false positives occurring. A possible solution could be to raise the detection threshold so that faces are only detected when the algorithm is confident to a high degree that the object detected is a face.

Epoch 7: This test illustrated the effect of false positives that have a large width and height. This can cause the drone to execute unpredictable movements.

Epoch 8: This test failed owing to the many face that were present in the video stream. This caused confusion in the algorithm and in turn caused the video stream from the drone to crash.

### Viola Jones Testing Summary

The drone performed tracking effectively using the Viola Jones algorithm. The main flaw of this algorithm was the occurrence of false positives. These false positives occurred in all areas of the video stream and caused the drone to erratically execute flight commands away from the tracking subject. This being said, an average of 54.52% of all frames in the video feed returned a true positive on the subjects detection. False positives occurred on average in 17.32% of all frames. Therefore the drone executed the correct tracking flight commands in 75.89% of all frames with a subject detected and executed incorrect flight commands in 24.10% of all frames with a subject detected.

## 6.4.2 CamShift Tracking Results

The following tests were performed using OpenCV and the CVDrone programming library. The video stream detects at an average of 15 frames per second. Tracking results are displayed in Table 6.28.

| Epoch # | Seconds | Total frames | # True positives | # False positives | % Overall detection | % True Positives | % False postives |
|---|---|---|---|---|---|---|---|
| 1 | 15 | 225 | 185 | 32 | 96.44% | 82.22% | 14.22% |
| 2 | 5 | 75 | 68 | 7 | 100.00% | 90.67% | 9.33% |
| 3 | 39 | 585 | 585 | 0 | 100.00% | 100.00% | 0.00% |
| 4 | 7 | 105 | 95 | 10 | 100.00% | 90.48% | 9.52% |
| 5 | 19 | 285 | 267 | 0 | 93.68% | 93.68% | 0.00% |
| 6 | 14 | 210 | 207 | 0 | 98.57% | 98.57% | 0.00% |
| 7 | 31 | 465 | 443 | 0 | 95.27% | 95.27% | 0.00% |
| 8 | 3 | 45 | 30 | 0 | 66.67% | 66.67% | 0.00% |
| 9 | 50 | 750 | 680 | 0 | 90.67% | 90.67% | 0.00% |
| 10 | 55 | 825 | 795 | 0 | 96.36% | 96.36% | 0.00% |
| 11 | 58 | 870 | 802 | 0 | 92.18% | 92.18% | 0.00% |
| 12 | 47 | 705 | 680 | 0 | 96.45% | 96.45% | 0.00% |

Table 6.28: CamShift Tracking Results

### Notes on each test Epoch

Epoch 1: Successful flight. False positives occurred briefly due to a red stapler entering the frame.

Epoch 2: The video feed crashed unexpectedly.

Epoch 3: Successful flight. No false detections. Altitude flight adjustments were disabled to allow for a more steady flight.

Epoch 4: The video stream was delayed in arriving at the client terminal and so tracking commenced mid-flight instead of at take-off. The drone successfully maintained a calculated distance from the subject and tracked the subject successfully. A false positive occurred on a pair of red shoes in the environment for a short time.

Epoch 5: Successful flight. Flight was slightly unstable as over corrections in altitude caused the drone to "bounce" up and down. The video stream crashed possibly owing to the drone activating "emergency mode" owing to unstable flight. Emergency mode cuts power to the engines and halts the reception and transmission of AT Commands, NavData and video stream.

Epoch 6: Again the video stream was late in arriving at the client terminal. However, once it started, tracking commenced with stability.

Epoch 7: Successful flight. The drone exhibited a "bounce" when executing the Yaw movement but stabilised after 3 seconds. Performed altitude adjustments smoothly.

Epoch 8: The drone cut power to the engines abruptly owing to batter power being low. The drone attempted to take off again but was unable to owing to a shift in the indoor hull that hindered the movement of the rotors.

Epoch 9: Successful flight. Recovered the image of the ball when the ball was removed from the video stream. Performed altitude adjustments smoothly.

Epoch 10: Successful flight. Maintained distance from object well. Exhibited bounce in the Yaw movement but corrected after 2 seconds.

Epoch 11: Successful flight. Maintained distance from object well. Exhibited bounce in the Yaw movement but corrected after 2 seconds.

Epoch 12: Successful flight. Maintained distance from object well. Exhibited bounce in the Yaw movement but corrected after 2 seconds.

### CamShift Testing Summary

The drone performed tracking extremely effectively using the CamShift algorithm. The main flaw of this algorithm was the occurrence of "bounce" in drone movements. This was owing to flight movements that over corrected the drone's position according to which quadrant the subject was in. This caused brief movements of instability during flight. A very low number of frames returned false positives and this only occurred when similarly coloured objects entered the frame. An average of 91.10% of all frames in the video feed returned a true positive on the subject's detection. False positives occurred on average in 2.76% of all frames. Therefore the drone executed the correct tracking flight commands in 97.06% of all frames with a subject detected and executed incorrect flight commands in 2.93% of all frames with a subject detected.

## 6.4.3 Fiducial Marker Tracking Results

The following tests were performed using the EZ-B robotics API. The video stream detects at an average of six frames per second. Tracking results are displayed in Table 6.29.

| Epoch # | Seconds | Total frames | # True positives | # False positives | % Overall detection | % True Positives | % False postives |
|---|---|---|---|---|---|---|---|
| 1 | 11 | 66 | 30 | 0 | 45.45% | 45.45% | 0.00% |
| 2 | 7 | 42 | 28 | 0 | 66.67% | 66.67% | 0.00% |
| 3 | 7 | 42 | 28 | 0 | 66.67% | 66.67% | 0.00% |
| 4 | 9 | 54 | 24 | 0 | 44.44% | 44.44% | 0.00% |
| 5 | 22 | 132 | 82 | 0 | 62.12% | 62.12% | 0.00% |
| 6 | 15 | 90 | 24 | 0 | 26.67% | 26.67% | 0.00% |
| 7 | 24 | 144 | 60 | 0 | 41.67% | 41.67% | 0.00% |
| 8 | 7 | 42 | 12 | 0 | 28.57% | 28.57% | 0.00% |
| 9 | 17 | 102 | 60 | 0 | 58.82% | 58.82% | 0.00% |
| 10 | 24 | 144 | 84 | 0 | 58.33% | 58.33% | 0.00% |
| 11 | 30 | 180 | 102 | 0 | 56.67% | 56.67% | 0.00% |
| 12 | 30 | 180 | 84 | 0 | 46.67% | 46.67% | 0.00% |
| 13 | 21 | 126 | 90 | 0 | 71.43% | 71.43% | 0.00% |

Table 6.29: Fiducial Marker Tracking Results

### Notes on each test Epoch

Epoch 1: The drone took off using marker 1 as programmed. The drone began executing a pre-programmed search pattern initiated by the recognition of marker 2. Crashed into furniture.

Epoch 2: The drone took off using marker 1 as programmed. The drone began to track marker 3 but the video stream crashed.

Epoch 3: The drone took off using marker 1 as programmed. The drone began to track marker 3 but the video stream crashed.

Epoch 4: The drone took off using marker 1 as programmed. The drone began executing a pre-programmed search pattern initiated by the recognition of marker 2. Crashed into furniture.

Epoch 5: The drone took off using marker 1 as programmed. The drone began tracking marker 3. Due to the delay in marker detection time, AT commands were being sent to the drone infrequently. This resulted in marker detection points in the video feed being far apart. Crashed into furniture.

Epoch 6: The drone is unable to detect or recognise markers beyond approximately 2m.

Epoch 7: Successful flight. However the algorithm struggles to pick up a marker moving faster than approximately 1m/s.

Epoch 8: Steady detection but crashed into furniture owing to the drones inertial movement.

Epoch 9: Successful flight. However, the grid tracking lines seem to be causing to the drone to execute rotation commands too sensitively for the distance that the fiducial marker can be tracked at.

Epoch 10: Successful flight. Performs rotation smoothly. Distance maintenance from the marker is miscalculating.

Epoch 11: Successful flight. Performs rotation smoothly. Distance maintenance from the marker is miscalculating.

Epoch 12: Successful flight. Performs rotation smoothly. Distance maintenance from the marker is miscalculating.

Epoch 13: Successful flight. Performs rotation smoothly. Performs altitude changes smoothly. Delay in marker detection evident.

### Fiducial Marker Testing Summary

The drone performed tracking erratically using the fiducial marker tracking algorithm. The main flaw of this algorithm was the delay in marker recognition. This affected the speed at which a moving marker could be recognised. The algorithm produced no false positives which ensured that only correct flight commands were executed. An average of 51.86% of all frames in the video feed

returned a true positive on the subject's detection. False positives occurred on average in 0.00% of all frames. Therefore the drone executed the correct tracking flight commands in 100% of all frames with a subject detected and executed incorrect flight commands in 0.00% of all frames with a subject detected.

### 6.4.4 Upper body Tracking Results

The following tests were performed using the EZ-B robotics API. The video stream detects at an average of six frames per second. Tracking results are displayed in Table 6.30.

| Epoch # | Seconds | Total frames | # True positives | # False positives | % Overall detection | % True Positives | % False postives |
|---|---|---|---|---|---|---|---|
| 1 | 10 | 60 | 42 | 6 | 80.00% | 70.00% | 10.00% |
| 2 | 13 | 78 | 57 | 15 | 92.31% | 73.08% | 19.23% |
| 3 | 10 | 60 | 40 | 15 | 91.67% | 66.67% | 25.00% |
| 4 | 16 | 96 | 66 | 22 | 91.67% | 68.75% | 22.92% |

Table 6.30: Upper Body Haar Cascade Tracking Results

#### Notes on each test Epoch

Epoch 1: Detects the upper body and tracking performs smoothly. As the drone gets closer to the subject the algorithm does not perform well as it needs approximately 2-4m from the subject to detect an upper body.

Epoch 2: Detects the upper body with a high accuracy but struggles to perform a turn. The confined testing environment limits the drones tracking rotation.

Epoch 3: Upper body detected. Crashed into furniture owing to inertial drone movement.

Epoch 4: Successful flight. Many false positives detected but tracking maintained.

#### Upper Body Testing Summary

The drone performed tracking effectively using the upper body Haar Cascade algorithm. The main flaw of this algorithm was the distance at which an upper body can be detected. As the drone approached the subject, detection was lost. This algorithm is effective at tracking from a distance. A small number of false positives occurred. At a distance of 2m from the subject these false positives can cause the drone to erratically execute flight commands as they occur in various quadrants. This being said, an average of 69.62% of all frames in the video feed returned a true positive on the subject's detection. False positives occurred on average in 19.29% of all frames. Therefore the drone

executed the correct tracking flight commands in 78.30% of all frames with a subject detected and executed incorrect flight commands in 21.69% of all frames with a subject detected.

## 6.5 Summary

The results from tests performed on the AR Drone were positive and highlighted many of the strengths and weaknesses that need to be considered when implementing a detection, recognition and tracking system for the drone. Many of the algorithms encountered problems with the detection of false positives and this impeded the drone's ability to track a subject completely accurately. There were limitations on the distances at which algorithms could successfully track their subjects. This limitation is a consequence many factors such as image pixel density, frame frequency and the lighting in a tracking environment. It is expected that the drone's capable tracking distances would increase by making use of a higher quality camera and algorithms with more elaborate detection techniques. The inertial movement of the drone caused some flight test results to vary especially owing to the small size of the testing environment. On a larger scale, the drone's inertial movement is expected to become negligible to an extent. The relatively few number of angle that subjects were able to be detected at required tests to be performed in fairly ideal conditions. Advanced searching algorithms could be employed to assess an environment at as many angles as possible to deal with this limitation. When performing recognition, there was a small amount of time needed to process a detected subject. This led to noticable delays in tracking command execution and limited the speed at which an object was able to move whilst successfully performing tracking. Toward the end of testing, the drone's components became slightly damaged from test flight crashes and made some flight movements unpredictable. The drone was successfully able to detect, recognise and track various subjects during tests and provided useful insight into the AR Drones capability and limitations.

# Chapter 7

# Conclusion

The system created performs the autonomous functions of target detection, recognition and tracking using the Parrot AR Drone. Various methods and algorithms were used to implement each function and the capability of these algorithms was tested rigorously. Each algorithms capable distance, angle of detection, accuracy and tracking performance was assessed to determine whether using a drone to perform these functions was conceptually feasible. Various strengths and limitations of the AR Drone and the algorithms used to implement each of the functions were identified. The AR Drone was the most suitable aerial vehicle to implement this system as it allowed each of the algorithms to be tested indoors in a controlled environment. This allowed the algorithms to be tested in an environment devoid of many outdoor factors such as wind, condensation and lighting changes. The AR Drones ability to hover made it possible to perform tests in a small and monitorable space which would not be possible using fixed wing drones.

The APIs that were used were chosen according to how well they implemented an algorithm. It was found that one API could implement a certain algorithm effectively but encountered difficulties with others. The tools, functions and programming languages of each API determined its capabilities and so different APIs were used to implement various algorithms.

A few challenges were encountered when implementing and testing algorithms. The video feed from the AR Drone would occasionally crash owing to the drone venturing too far from the client PC or from socket exceptions. The socket exceptions caused the existing video feed connection to the drone to be closed by the remote host and so the visual capabilities of the drone were periodically lost. The drone's components became slightly damaged towards the end of testing which caused drone to move unpredictable at times.

The results obtained from testing showed that the Camshift and Viola Jones face detection algorithms were the most effective in terms of distance capabilities, effective detection angles, accuracy and tracking performance. Fiducial marker recognition allowed the drone to effectively execute predefined flight scripts but was not able to recognise markers from distances beyond approximately 2m. The Haar-Cascade algorithms performed relatively well with the exception of the eye detection which produced very ineffective test results. Fisherfaces was able to recognise a face with relative accuracy but this accuracy declined rapidly as the sample set of trained faces became larger.

The system was successfully able to evaluate the capabilities of various algorithms and demonstrated that a micro UAV such as the Parrot AR Drone is capable of performing autonomous detection, recognition and tracking during flight. The requirements detailed in Chapter 1 are deemed to have been successfully fulfilled.

## 7.1 Future Work

One could elaborate on this system in various ways. Firstly, one could make use of a camera that can capture video at a higher pixel density and frame rate. This would increase the accuracy of detection as well as the distance of detection. Objects that are detected at a distance could be zoomed in on for more accurate tracking and recognition. To further improve the detection and tracking capabilities of the drone, a function could be created that selects the most appropriate tracking algorithm according to the drones environment. The drone could attempt to detect a human initially by using face detection. Should this prove unsuccessful the drone could swap to an upper body or full body Haar Cascade detection algorithm. The would enable the drone to constantly swap between algorithms to maintain a lock on the target.

3D mapping could be used to create an image of the immediate environment so that the drone could autonomously navigate around obstacles on its flight path whilst tracking a target. Currently the drone requires a client application to perform image processing and send flight commands. The drone communicates with this client application via Wi-Fi and so there is a limit on how far the drone can travel from its client device. Placing an on board computer such as the Raspberry Pi on the drone would eliminate this limitation. Finally, the AR Drone is only able to operate outdoors in clam weather conditions. A more robust drone design would be needed for the drone to handle strong winds or rain. A more robust drone such as a hexrotor could be used to handle these conditions. This would also allow the drone to carry a heavier payload such as additional batteries, sensors and on board computer.

# Bibliography


Achtelik, Markus, Bachrach, Abraham, He, Ruijie, Prentice, Samuel, & Roy, Nicholas. 2009. Stereo vision and laser odometry for autonomous helicopters in GPS-denied indoor environments. *In: SPIE Defense, Security, and Sensing*. International Society for Optics and Photonics.

Allen, John G, Xu, Richard YD, & Jin, Jesse S. 2004. Object tracking using camshift algorithm and multiple quantized feature spaces. *Pages 3–7 of: Proceedings of the Pan-Sydney area workshop on Visual information processing*. Australian Computer Society, Inc.

AR.Drone. 2009. ARDrone API. Online. Available from: `https://projects.ardrone.org/`. Accessed on 31 Oct 2013.

AR.Drone2.0. 2013. Repair Your AR.Drone. Online. Available from: `http://ardrone2.parrot.com/repair-your-ardrone/`. Accessed on 31 Oct 2013.

Arjomandi, Maziar, Agostino, S, Mammone, M, Nelson, M, & Zhou, T. 2007. Classification of Unmanned Aerial Vehicles. *The University of Adelaide, Australia*.

Beard, Randal W, Kingston, Derek, Quigley, Morgan, Snyder, Deryl, Christiansen, Reed, Johnson, Walt, McLain, Timothy, & Goodrich, Michael. 2005. Autonomous vehicle technologies for small fixed-wing UAVs. *Journal of Aerospace Computing, Information, and Communication*, **2**(1), 92–108.

Belhumeur, Peter N., Hespanha, João P, & Kriegman, David J. 1997. Eigenfaces vs. fisherfaces: Recognition using class specific linear projection. *IEEE Transactions on Pattern Analysis and Machine Intelligence*, **19**(7), 711–720.

Belisarius. 2011. Image Segmentation using Mean Shift explained. Online. Available from: `http://stackoverflow.com/questions/4831813/image-segmentation-using-mean-shift-explained`. Accessed on 31 Oct 2013.

Biber, Peter, Andreasson, Henrik, Duckett, Tom, & Schilling, Andreas. 2004. 3D modeling of indoor environments by a mobile robot with a laser scanner and panoramic camera. *Pages 3430–3435 of: Proceedings IEEE/RSJ International Conference on Intelligent Robots and Systems.(IROS 2004).*, vol. 4. IEEE.

Bills, Cooper, Chen, Joyce, & Saxena, Ashutosh. 2011. Autonomous MAV flight in indoor environments using single image perspective cues. *Pages 5776–5783 of: IEEE international conference on Robotics and automation (ICRA 2011).* IEEE.

Bradski, Gary R. 1998. Real time face and object tracking as a component of a perceptual user interface. *Pages 214–219 of: Proceedings of IEEE Workshop on Applications of Computer Vision (WACV 1998).* IEEE.

Bristeau, Pierre-Jean, Callou, François, Vissière, David, Petit, Nicolas, *et al.* 2011. The Navigation and Control technology inside the AR.Drone micro UAV. *Pages 1477–1484 of: World Congress*, vol. 18.

Cambridge, AT&T Laboratories. 2002. The Database of Faces. Online. Available from: `http://www.cl.cam.ac.uk/research/dtg/attarchive/facedatabase.html`. Accessed on 8 Aug 2013.

Çelik, Koray, Chung, Soon-Jo, Clausman, Matthew, & Somani, Arun K. 2009. Monocular vision SLAM for indoor aerial vehicles. *Pages 1566–1573 of: IEEE/RSJ International Conference on Intelligent Robots and Systems. (IROS 2004).* IEEE.

Cherian, Anoop, Andersh, Jonathan, Morellas, Vassilios, Papanikolopoulos, Nikolaos, & Mettler, Bernard. 2009. Autonomous altitude estimation of a UAV using a single onboard camera. *Pages 3900–3905 of: IEEE/RSJ International Conference on Intelligent Robots and Systems. (IROS 2009).* IEEE.

Courbon, Jonathan, Mezouar, Youcef, Guenard, Nicolas, & Martinet, Philippe. 2009. Visual navigation of a quadrotor aerial vehicle. *Pages 5315–5320 of: IEEE/RSJ International Conference on Intelligent Robots and Systems.(IROS 2009).* IEEE.

Crew, Flight. 2013. Flight Crew-Fixed Wing Vs Rotary UAV. Online. Available from: `http://www.hse-uav.com/fixed_wing_vs_rotary_wing_uav.htm`. Accessed on 19 May 2013.

Danko, Todd W, Kellas, Andreas, & Oh, Paul Y. 2005. Robotic rotorcraft and perch-and-stare: sensing landing zones and handling obscurants. *Pages 296–302 of: Proceedings of the 12th International Conference on Advanced Robotics.(ICAR 2005).* IEEE.

de Souza, Cesar. 2012. Haar-feature Object Detection in C. Online. Available from: http://www.codeproject.com/Articles/441226/Haar-feature-Object-Detection-in-Csharp. Accessed on 31 Oct 2013.

Dijkshoorn, Nick. 2012. *Simultaneous localization and mapping with the ar. drone.* Ph.D. thesis, Universiteit van Amsterdam.

Greensted, Dr. Andrew. 2010. Otsu Thresholding. Online. Available from: http://www.labbookpages.co.uk/software/imgProc/otsuThreshold.html. Accessed on 31 Oct 2013.

Hewitt, Robin. 2007. Face Recognition With Eigenface. Online. Available from: http://www.cognotics.com/opencv/servo_2007_series/part_4/page_2.html. Accessed on 31 Oct 2013.

Hwang, Wonjun, Kim, Tae-Kyun, & Kee, Seokcheol. 2004. LDA with subgroup PCA method for facial image retrieval. *Pages 21–23 of: The 5th International Workshop on Image Analysis for Multimedia Interactive Services (WIAMIS 2004).*

Isaac Gerg, Adam Ickes, Jamie McCulloch. 2003. CamShift Tracking Algorithm. Online. Available from: http://www.gergltd.com/cse486/project5/. Accessed on 31 Oct 2013.

Johnson, Neil G. 2008. *Vision-assisted control of a hovering air vehicle in an indoor setting.* Ph.D. thesis, Brigham Young University. Department of Mechanical Engineering.

Kendoul, Farid, Fantoni, Isabelle, & Nonami, Kenzo. 2009. Optic flow-based vision system for autonomous 3D localization and control of small aerial vehicles. *Robotics and Autonomous Systems*, **57**(6), 591–602.

Kirillov, Andrew. 2010. Glyph's recognition. Online. Available from: http://www.aforgenet.com/articles/glyph_recognition/. Accessed on 31 Oct 2013.

Mayer, Jane. 2009. The predator war. *The New Yorker*, **85**, 36–45.

Mejias, Luis, Campoy, Pascual, Usher, Kane, Roberts, Jonathan, & Corke, Peter. 2006. Two seconds to touchdown-vision-based controlled forced landing. *Pages 3527–3532 of: IEEE/RSJ International Conference on Intelligent Robots and Systems.* IEEE.

Moore, Richard James Donald, Thurrowgood, Saul, Bland, Daniel, Soccol, Dean, & Srinivasan, Mandyam V. 2009. A stereo vision system for UAV guidance. *Pages 3386–3391 of: IEEE/RSJ International Conference on Intelligent Robots and Systems.(IROS 2009).* IEEE.

Mori, Ryosuke, Hirata, Kenichi, & Kinoshita, Takuya. 2007. Vision-based guidance control of a small-scale unmanned helicopter. *Pages 2648–2653 of: IEEE/RSJ International Conference on Intelligent Robots and Systems.(IROS 2007)*. IEEE.

Morris, Stephen J. 1997. Design and flight test results for micro-sized fixed-wing and VTOL aircraft. *In: Proceedings of the First Internation Conference on Emerging Technologies for Micro Air Vehicles, Atlanta, GA*. Citeseer.

Nicoud, J-D, & Zufferey, J-C. 2002. Toward indoor flying robots. *Pages 787–792 of: IEEE/RSJ International Conference on Intelligent Robots and Systems.*, vol. 1. IEEE.

OpenCV. 2013a. OpenCV Haar-Cascades. Online. Available from: `https://opencvlibrary.svn.sourceforge.net/svnroot/opencvlibrary/tags/latest_tested_snapshot/opencv/data/haarcascades`. Accessed on 31 Oct 2013.

OpenCV. 2013b. OpenCV Software Library. Online. Available from: `http://opencv.org`. Accessed on 31 Oct 2013.

Portal, João Víctor. 2011. *A Java autopilot for parrot AR drone designed with DiaSpec*. M.Phil. thesis, Universidade Federal Do Rio Grande Do Sul.

puku0x. 2012. CV Drone. Online. Available from: `https://github.com/puku0x/cvdrone`. Accessed on 31 Oct 2013.

Roberts, James F, Stirling, Timothy S, Zufferey, J-C, & Floreano, Dario. 2009. 2.5 D infrared range and bearing system for collective robotics. *Pages 3659–3664 of: IEEE/RSJ International Conference on Intelligent Robots and Systems.(IROS 2009)*. IEEE.

Soundararaj, Sai Prashanth, Sujeeth, Arvind K, & Saxena, Ashutosh. 2009. Autonomous indoor helicopter flight using a single onboard camera. *Pages 5307–5314 of: IEEE/RSJ International Conference on Intelligent Robots and Systems, 2009. (IROS 2009)*. IEEE.

Stephane Piskorski, Nicolas Brulez, Pierre Eline. 2011. *AR.Drone Developer Guide SDK 1.7*. Sdk 1.7 edn. Parrot.

Sures, DJ. Online. Available from: `http://www.ez-robot.com/EZ-Builder/`. Accessed on 31 Oct 2013.

Tournier, Glenn P, Valenti, Mario, How, Jonathan P, & Feron, Eric. 2006. Estimation and control of a quadrotor vehicle using monocular vision and moire patterns. *Pages 21–24 of: Navigation and Control Conference and Exhibit on AIAA Guidance*.

Turk, Matthew, & Pentland, Alex. 1991. Eigenfaces for recognition. *Journal of cognitive neuroscience*, **3**(1), 71–86.

Viola, Paul, Jones, Michael J, & Snow, Daniel. 2005. Detecting pedestrians using patterns of motion and appearance. *International Journal of Computer Vision*, **63**(2), 153–161.

Wagner, Philipp. 2012. Face Recognition with Python. Online. Available from: `http://www.bytefish.de/blog/fisherfaces/`. Accessed on 31 Oct 2013.

Zingg, Simon, Scaramuzza, Davide, Weiss, Stephan, & Siegwart, Roland. 2010. MAV navigation through indoor corridors using optical flow. *Pages 3361–3368 of: Robotics and Automation (ICRA), 2010 IEEE International Conference on*. IEEE.